1661-8726/08/020341-20
DOI 10.1007/s00015-008-1264-2
Birkhäuser Verlag, Basel, 2008

Swiss J. Geosci. 101 (2008) 341–360

Strain localization in the Morcles nappe (Helvetic Alps, Switzerland)

Nicholas Austin[1,*], Brian Evans[1], Marco Herwegh[2] & Andreas Ebert[2]

Key words: rheology, calcite, localization, recrystallization, microstructure, crystallographic preferred orientation

ABSTRACT

Deformation in orogenic belts is frequently accommodated in calcite-rich lithologies, owing to their relatively low strength, particularly compared to quartz-rich rocks. Here, we investigate the coupling between calcite grain size, the presence and mineralogy of second phases, and crystallographic preferred orientation (CPO) in a transect through deformed limestones, perpendicular to the dominant foliation in the inverted limb of the Morcles nappe of the Swiss Helvetic Alps. Calcite grain size becomes progressively finer as the thrust contact is approached, and there is a concomitant increase in CPO intensity, with the strongest CPO's in the finest-grained, quartz-rich limestones, nearest the thrust contact. To understand the distribution of strain and the extent of strain localization, we compared the paleowattmeter and calcite flow laws from laboratory studies to previously published observations of microstructure at a range of locations, with varying peak metamorphic temperatures, along the Morcles nappe. The strain-rates predicted by extrapolation of these laboratory relationships agree well with the geologic constraints. We then applied the same approach to the samples from the present study. The results indicate that strain became progressively localized towards the thrust contact of the Morcles nappe, leading to an increase in strain rate of >1 order of magnitude in a zone <0.50 m thick. For localization to occur system and/or material softening is necessary. If dislocation activity is positively correlated with CPO, then softening cannot have occurred by a complete transition to diffusion creep in the finest grained samples. Rather, softening may have resulted from the formation of CPO, possibly coupled with effects related to the distribution of second phases and the overall geometry of the shear zone.

1 Introduction

Inelastic strains in lithospheric rocks, deformed during tectonic processes, are often accommodated along narrow faults and shear zones. For example, geodetic data show that global strains are largely accommodated along a few localized features (Kreemer et al. 2000; Kreemer et al. 2003). Similarly, at the field scale, structural geologists often conclude that lateral displacements of up to several kilometers have been accommodated in shear zones with widths of centimeters to meters (Boullier & Quenardel 1981; Milton & Williams 1981; Harris et al. 1983; Siddans 1983; Groshong Jr et al. 1984). Thus, the mechanics of shear zones are an important element in geodynamics (Poirier 1980; Hobbs et al. 1990; Burg 1999; Rutter 1999; Montesi & Zuber 2002; Burlini & Bruhn 2005).

Owing to the relatively low strength of calcite-rich rocks, deformation during orogenic events is frequently localized within limestones and marbles, particularly where these lithologies are juxtaposed with quartz- and feldspar-rich rocks (Groshong Jr et al. 1984; Pfiffner 1993; Kennedy & White 2001). The Helvetic zone in western Switzerland is a useful location for investigating the rheology of naturally deformed limestones. The nappes that comprise this region are composed of Jurassic to Cretaceous sediments that Burkhard (1988) attributed to basins within the Alpine Tethys, which were closed and inverted during the Alpine orogeny, resulting in the formation of highly localized shear zones in the limestones of the overturned limbs of the nappes.

Motivated by the regional scale observations of Ebert et al. (2007a), in this study, we undertook a dense and systematic sampling of calcite mylonites in an ~12 m section of the inverted limb of Morcles nappe, in the Helvetic Alps of Switzerland near Saillon, just above the thrust contact with the autochthonous cover of the Aiguille Rouge Massif (Fig. 1). Earlier studies provide substantial constraints on the stratigraphy, geometry, and deformation history of the Morcles nappe and its eastern pen-

[1] Department of Earth, Atmospheric, and Planetary Sciences, Massachusetts Institute of Technology, Cambridge, MA, 02139, USA.
[2] Institute of Geological Sciences, Bern University, CH-3012 Bern, Switzerland.
*Corresponding author: N. Austin. E-mail: naustin@mit.edu

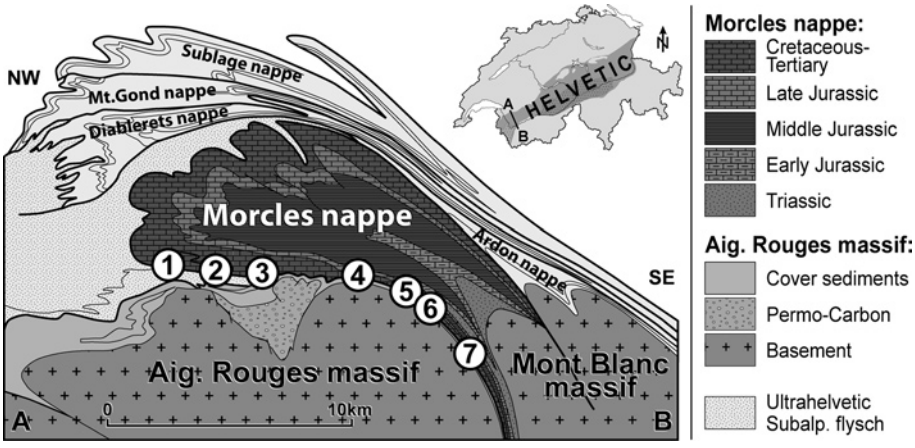

Fig. 1. A schematic cross section along transect A-B, from the map in the upper right hand corner, through the Helvetic nappes in southwestern Switzerland (after Escher et al. 1993 and Ebert et al. 2007a). Numbers correspond to sample locations from Ebert et al. (2007a). This study focuses on sample location 5 (Swiss Coordinates 578.950/113.500).

dant, the Doldenhorn nappe, at a regional scale (Badoux 1972; Ramsay 1981; Ramsay et al. 1983; Dietrich & Durney 1986; Burkhard & Kerrich 1988; Coward & Dietrich 1989; Dietrich & Casey 1989; Ramsay 1989; Escher et al. 1993; Pfiffner 1993; Crespo-Blanc et al. 1995; Kirschner et al. 1995; Kirschner et al. 1996; Burkhard & Goy-Eggenberger 2001; Bucher et al. 2003; Herwegh & Pfiffner 2005). Detailed studies of the microstructures of deformed marbles from a range of locations along the nappe also exist (Schmid et al. 1981; Dietrich 1986; Ebert et al. 2007a) (Figs. 1,2). Laboratory and field studies provide further insight into the coupling between strength and such microstructural elements as grain size and crystallographic preferred orientation (CPO) (Herwegh et al. 1997; Pieri et al. 2001a; Barnhoorn et al. 2004; Herwegh et al. 2005). By observing the matrix microstructure, matrix CPO, and the geometry and distribution of second phases at this particular location, we aim to identify and constrain the deformation mechanisms that operated, and to understand the spatial and temporal distribution of strain and strain rate in the shear zone.

2 Regional geology

The Helvetic nappes in western Switzerland are a stack of folds that include, moving structurally upwards, the Morcles, the Diablerets, and the Wildhorn nappes. This stack, in turn, is overlain by the Ultrahelvetic nappes (Escher et al. 1993). The Helvetic nappes were emplaced from top to bottom, and, thus, the thrust surfaces of the upper folds were bent during the emplacement of the lower ones (Trümpy 1973; Ramsay 1981). The Morcles nappe, itself, is a NW-verging recumbent fold, consisting primarily of Jurassic and Cretaceous shallow-water limestones with intercalated shales and marls (Badoux 1972; Epard 1990). The lower limb of this fold was inverted during the Alpine orogeny (Pfiffner 1981; Ramsay 1981, 1989; Pfiffner 1993). During the period from early Oligocene to Miocene, the recumbent-fold structure, which roots in the Mont Blanc massif, was thrust >10 km over the Aiguille Rouge Massif and its cover of siliciclastic sediments and flysch units (Goy-Eggenberger 1998). The overturned limb of the nappe has been extensively sheared, resulting in axial ratios up to and exceeding 90:1 (Badoux 1972; Ramsay 1981; Siddans 1983; Dietrich 1989; Dietrich & Casey 1989; Kirschner et al. 1996). In addition, there was a late stage of brittle faulting and kinking associated with uplift. The total displacement accommodated in the inverted limb of the Morcles nappe varies from a maximum of 10–12 km in the root zone, to zero at the front of the nappe (Pfiffner 1993; Panien et al. 2005; Ebert et al. 2007a).

The peak metamorphic temperature at the toe of the nappe was approximately 200 °C, with temperatures increasing linearly down-dip to greater than 350 °C in the root zone (Frey et al. 1980; Kirschner et al. 1995; Burkhard & Goy-Eggenberger 2001; Ebert et al. 2007a) (Fig. 2). Folding of the sediments began before diagenesis was complete, resulting in the expulsion of significant volumes of fluids (Kirschner et al. 1995). Rapid burial to depths of 6–8 km occurred between 29 and 24 Ma, producing peak metamorphic conditions, which were accompanied by northward thrusting (Loup 1992; Kirschner et al. 1999). As the nappe deformed, the shear zone narrowed, resulting in a highly localized region of deformation (Ramsay et al. 1983), accommodated, wholly or in part, by crystal-plastic mechanisms (Schmid et al. 1981; Dietrich 1986; Ebert et al. 2007a), until ~16 Ma. Thermal modeling suggests that temperatures dropped by ~30–50 °C during thrusting (Kirschner et al. 1995; Kirschner et al. 1996), and the last stages of deformation, during exhumation, were probably accommodated by brittle faulting (Burkhard & Kerrich 1988; Herwegh & Pfiffner 2005). Some fluids flowed along the thrust contact during deformation, but there is little evidence of fluid transport within the internal portions of the nappe (Kirschner et al. 1999).

3 Outcrop-scale structures

Three distinct lithologies outcrop at the study location (Swiss Coordinates 578.950/113.500), where the peak metamorphic temperature has been estimated as 358 ± 15 °C (Dietrich & Casey 1989; Marquer et al. 1994; Kirschner et al. 1995; Burkhard & Goy-Eggenberger 2001; Ebert et al. 2007a) (Figs. 1–3). The structurally highest lithology considered here is the limestone

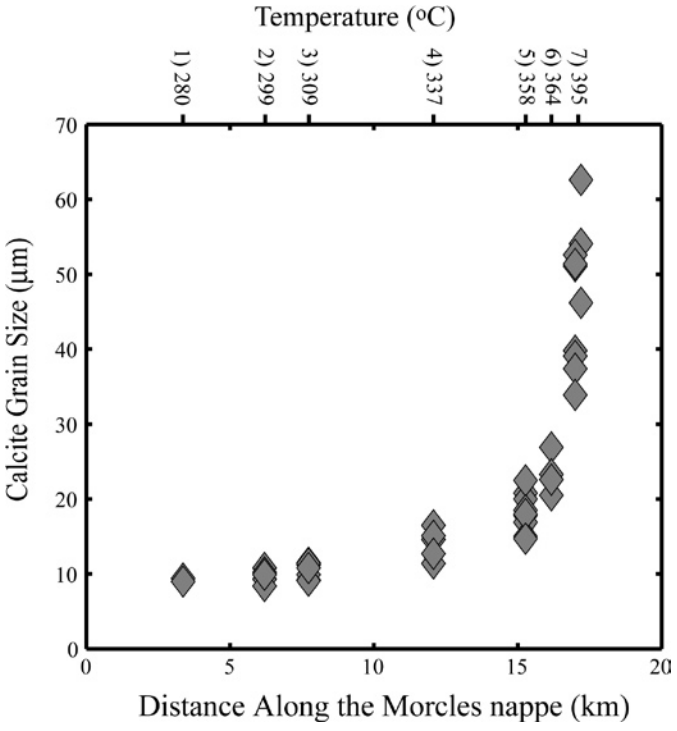

Fig. 2. The variation in grain size and temperature along the inverted limb of the Morcles nappe, using data from Ebert et al. (2007a). The numbers preceding temperatures correspond to the locations highlighted in figure 1.

of the lower Urgonian. Rocks in this formation are gray and, on average, consist of greater than 95 vol% calcite. Below this unit are outcrops of upper Urgonian limestone, ~5 m thick, containing greater than 95 vol% calcite, which are distinguished from the lower Urgonian by their white colour. Structurally below this is a section of Gault limestone, >7 m thick, green in colour, and containing up to 50 vol% quartz and chlorite. The autochtonous Triassic cover sediments of the Aiguille Rouge massif do not outcrop at this location. Throughout the study area, stratigraphic layering is parallel to the dominant foliation, which dips at 35–40º towards the ESE.

Oblique to the main foliation are progressive generations of meso-scale shear zones (denoted by "loc" in Table 1), resulting in imbrication of (a) lower Urgonian and upper Urgonian (Fig. 3b, c), and (b) upper Urgonian and Gault (Fig. 3d). Progressive generations of these features cross-cut each other (Fig. 3b, c), and are associated with isoclinal folding of the main foliation (Fig. 3c), indicating that these features formed while distributed deformation was still occurring throughout the shear zone, and thus, are probably not related to brittle deformation associated with uplift.

4 Microstructures within the Morcles nappe

Heavily sheared marbles in the lower limb of the Morcles nappe show clear evidence that crystal-plastic mechanisms operated (Ramsay 1981; Schmid et al. 1981; Ramsay et al. 1983; Dietrich & Song 1984; Dietrich 1986; Ebert et al. 2007a): coarse vein calcite is heavily twinned and recrystallized; matrix calcite exhibits elongation (Schmid et al. 1981) and shows characteristic recrystallization microstructures (Ebert et al. 2007a). In addition, near the thrust contact, the matrix calcite contains a distinct CPO, with c-axes oriented normal to the main foliation, which parallels the shear-zone boundary, consistent with formation during shear, rather than during initial folding (Schmid et al. 1981; Dietrich 1986; Ebert et al. 2007a). Calcite grain sizes decrease non-linearly from the root zone of the Morcles nappe to the fold hinge, even when there is no evidence that additional phases influence the matrix grain size (Ebert et al. 2007a). In addition, CPO intensity decreases as peak temperature decreases. The presence of second phases (i.e. minerals other than calcite) results in reduced matrix grain size, but this effect is more pronounced for samples containing sheet silicates than for those containing rounded quartz grains (Ebert et al. 2007a). CPO is also weaker in samples containing large volume fractions of second phases (Ebert et al. 2007a). Those authors found elevated dislocation densities in calcite grains in the vicinity of sheet silicates, in samples with a weak CPO, compared to calcite grains distal to sheet silicates in rocks with strong CPO.

5 Methodology of new observations

Sampling

Specimens were collected along a transect normal to the primary foliation, over a distance of 12.55 m. When heterogeneity in the formation existed, additional samples were selected from regions that were cut by the meso-scale shear zones or that contained anomalously high or low second-phase contents, to supplement those from nearby regions apparently homogeneously deformed. In total, 27 samples have been analyzed as part of this study (Table 1). Although the autochthonous Triassic cover of the Aiguille Rouge Massif does not outcrop at the study location, we believe that the structurally lowest sample (MOG18N1) is $\ll$1 m from the contact between the inverted limb of the Morcles nappe and the Triassic, based on the thickness of Gault at this location and on the foliation intensity of that sample. All distances are given relative to sample MOG18N1, and are considered estimated distances to the thrust contact. Oriented sections were prepared parallel to the dominant lineation and perpendicular to the primary foliation (i.e. the shear plane), and were etched in dilute hydrochloric acid and acetic acid in order to highlight grain boundaries and create relief between the calcite grains and second phases (Herwegh 2000).

Grain size and second-phase content

Calcite grain sizes were determined using the linear-intercept method on reflected-light micrographs of the oriented, etched samples. Average intercept lengths were measured both parallel and perpendicular to the foliation. A factor of 3/2 was used to

Table 1. Sample names; distance from MOG18N1 normal to the thrust contact, which we considered the estimated distance to the thrust contact; average calcite grain size from linear intercept measurements (D_{cc}), including a stereological correction of 3/2; mineralogy of second phases in the given lithology (usual abbreviations, Sh.Sil refers generically to sheet silicates), and the M-Index (Skemer et al. 2005) from crystallographic orientations obtained by EBSD. All samples are from the Saillon cave (Swiss Coordinates 578.950/113.500). Lithology is given in the sample name: MOG refers to the Gault, MOU refers to the upper Urgonian, and MOUg refers to the lower Urgonian. Zones of apparent localization, including the boundaries of the meso-scale shear zones are denoted with "loc".

Sample	Distance relative to MOG18N1 (m)	Dcc (μm)	Z (μm)	Second Phases	M-Index (calcite)
MOG18N1	0.00	4.3–8.9	38-pure	Qtz	0.19–0.49
MOG18N2	0.25	9.5–10.3	43-pure	Qtz + Chl	0.10
MOG18N3	0.75	13.3–15.1	460-pure	Qtz + Chl	0.11
MOG18N4	1.05	6.5	69	Qtz + Chl	0.15
MOG18N5	1.35	10.1–11.1	47–72	Qtz + Chl	0.09
MOG18N6	2.25	11.3–11.4	67–142	Qtz + Chl	
MOG18N7t	2.75	12.0–12.7	146–206	Qtz + Chl	
MOG18N8	4.85	14.5–15.9	73–101	Qtz + Chl	
MOG18N9	5.65	20.6–22.0	pure		0.21
MOG18N10t	7.25	14.3–17.2	778–895	Qtz + Chl	
MOU18N18	7.60	22.4	pure		
MOU18N19	7.63	22.5–24.1	pure		
MOU18N21t	7.95	14.5–21.6	85-pure	Sh.Sil +/– Qtz	
MOU18N22	8.65	19.6–20.8	1776-pure	Sh.Sil +/– Qtz	0.14
MOU18N22 loc	8.65	7.6–9.9	58–441	Sh.Sil +/– Qtz	0.07
MOU18N23	8.65	20.6–24.6	pure		0.14
MOU18N23 loc	8.65	7.5	86	Sh.Sil +/– Qtz	0.04
MOU18N11	8.90	23.2–25.1	pure		0.08
MOU18N25	9.35	21.9	pure		
MOU18N12	9.50	19.2–21.5	pure		
MOU18N14	9.50	15.6–21.8	169-pure	Sh.Sil +/– Qtz	0.16
MOU18N24	9.65	18.1	pure		
MOU18N13t	10.00	15.4–20.8	125-pure	Sh.Sil +/– Qtz	0.09
MOU18N15	10.00	14.6–23.6	236-pure	Sh.Sil +/– Qtz	
MOU18N27t	10.25	21.1–26.5	pure		
MOU18N17t	10.30	14.5–23.2	86-pure	Sh.Sil +/– Qtz	
MOU18N30	11.05	13.9–20.8	110-pure	Sh.Sil +/– Qtz	0.04
MOU18N30 loc	11.05	11.8–14.7	79-pure	Sh.Sil +/– Qtz	
MOU18N28b	11.25	18.5–21.3	272-pure	Sh.Sil +/– Qtz	
MOUg18N29	12.55	18.1–26.2	73-pure	Sh.Sil +/– Qtz	0.16

correct the average intercepts (Underwood 1970; Exner 1972). The average grain sizes we obtained using this technique are consistent with those obtained by area weighting equivalent circular diameters of measured grain areas on samples from the outcrop we are investigating (Ebert et al. 2007a). The size and area of second-phase grains were determined by tracing regions of high relief, as observed in reflected light, and measuring the tracings using NIH ImageJ®. When second-phase grains were in direct contact, they were treated as a single grain, because we were primarily interested in the influence of second phases in pinning matrix grain boundaries. We characterized the dispersion of second phases by calculating a Zener parameter (Z) (Smith 1948; Nes et al. 1985; Olgaard & Evans 1986; Humphreys & Ardakani 1996)

$$Z = \frac{d_2}{f_2^k} \quad (1)$$

Here, d_2 refers to the grain or aggregate size of second phases, and f_2 refers to the areal fraction of those phases. The exponent, k, varies between 0.33 and 1 depending on details of the

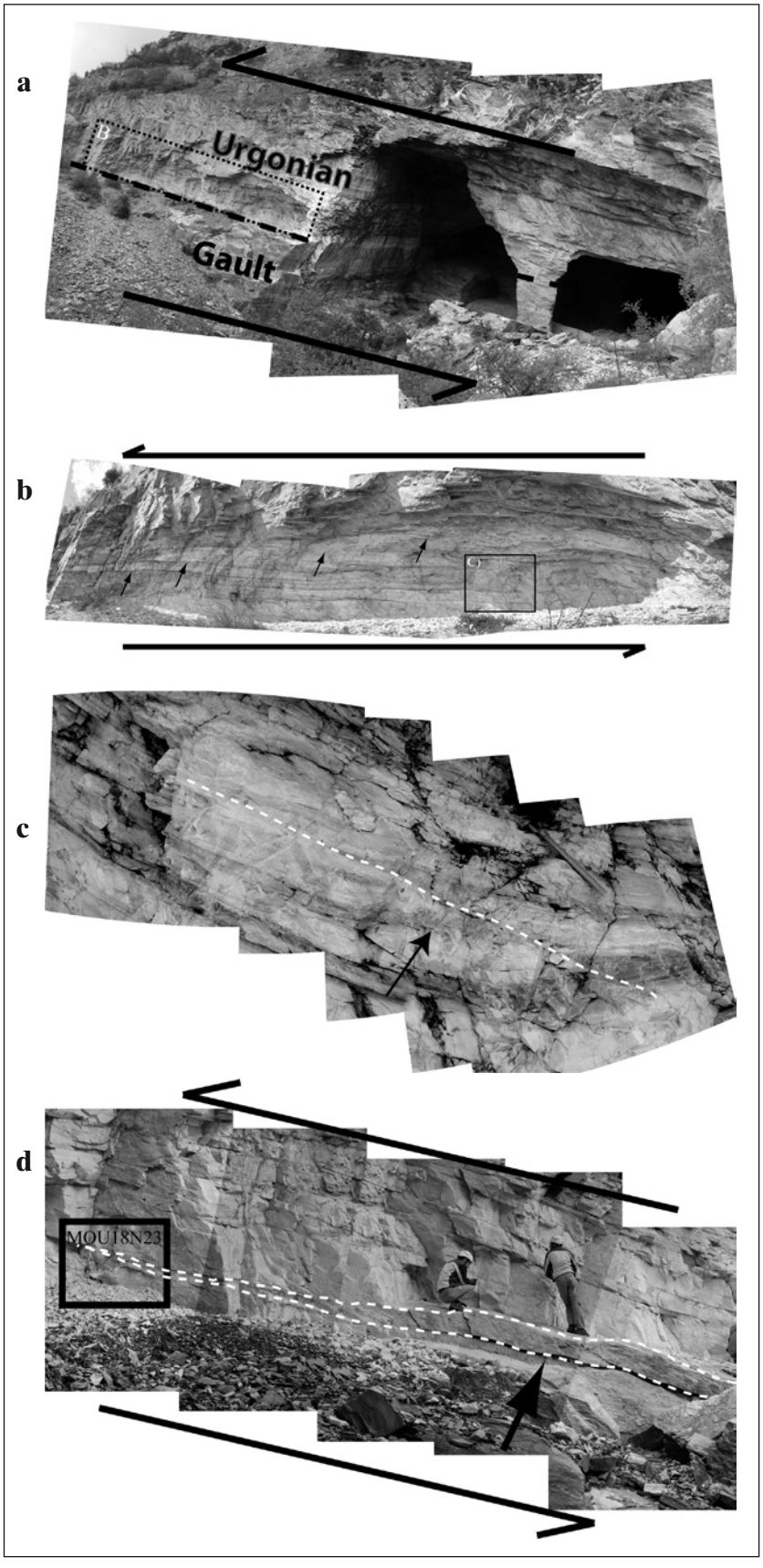

Fig. 3. A) The outcrop (location 5 in figure 1) where all the samples were obtained for this study. The lithological contact between the Gault and the Urgonian, which parallels the shear-zone boundary, is highlighted. The lowermost sample (MOG18N1) was taken from the back of the cave, at the lower right of image, and the uppermost sample (MOUg18N29) was taken from the outcrop near the bushes in the upper left of the image. These two locations are separated by a distance of 12.55 m normal to the thrust contact. The dashed box highlights the region shown in figure 3b. B) The contact between the upper Urgonian (white) and the lower Urgonian (grey). Notice the discrete bands of lower Urgonian within the upper Urgonian (highlighted with arrows). The box corresponds to the location of figure 3c. C) Evidence of the contemporaneous activity of folding (see arrow) and localized shear (white dashed line) (hammer for scale). D) A band of Gault (highlighted with white dashed lines) imbricated into the upper Urgonian. The box shows the location of samples MOU18N22 and MOU18N23 (human for scale).

dispersion of pinning phases. Based on extensive microstructural observations, Ebert et al. (2007a) suggested that $k = 1$ is the appropriate exponent for calcite mylonites in the Morcles nappe. But even withstanding that conclusion, Z should serve as a relative measure of the dispersion of the second phases, for which purpose it is used here. Second-phase mineralogy was determined by observation in both transmitted and reflected light. Wherever possible, observations were made in adjacent bands of nominally "pure" and "impure" matrix.

Analysis of crystallographic preferred orientation

Crystallographic preferred orientation (CPO) was measured by Electron Back Scatter Diffraction (EBSD) on the oriented sections previously used for measurement of matrix grain size and second-phase content. In many samples, several areas within a given section were analyzed for both CPO and grain size. Analyses were performed using a JEOL JSM 840 SEM with HKL Channel 5+ software at the Woods Hole Oceanographic Institution (WHOI), with an accelerating voltage of 15 kV, tilt of 70º, and working distance of 23 mm. The beam current was varied between 3e-7 and 3e-8 A. For each region of investigation, ~200 individual grains were manually selected by ensuring that the diffraction pattern was significantly different than neighboring analyses. Each analysis was indexed using the HKL software, accepting only fits with a mean angular deviation (MAD) < 1.3. In addition, each indexed pattern was manually checked. Analyses from 200 individual grains have been shown to be sufficient to quantify texture intensity (Skemer et al. 2005). Several samples were also analyzed using a Zeiss EVO 50 SEM with TSL-EBSD system (OIM 4.5 software) and automated data acquisition of >1000 points (step sizes 1–5 μm), at the University of Bern. The resulting crystallographic orientations were indistinguishable from those obtained manually at WHOI. Pole figures were created using the program PFch5 (D. Mainprice, pers. comm., 2007). They are presented as lower hemisphere projections with Gaussian smoothing of 8.5º, and are contoured for each multiple of a uniform distribution (MUD) up to global maximum of 15. The texture intensity is quantified with the M-Index (Skemer et al. 2005).

6 Microstructural observations

Matrix grain size

Three distinct trends in grain size are observed in the deformed marbles in the inverted limb of the Morcles nappe (Figs. 4–6). Most striking is the reduction in calcite grain size (D_{cc}) with decreasing distance to the thrust contact (Fig. 6a). Secondly, it is well known that second-phase content may influence the matrix grain size, and this effect has been copiously documented in naturally deforming rocks (Mas & Crowley 1996; Krabbendam et al. 2003; Herwegh & Berger 2004; Herwegh et al. 2005; Ebert et al. 2007a; Ebert et al. 2007b). In this study, samples from all three units appear to cluster into one of two groups, those with Z greater than or less than 500 μm, respectively (Fig. 6). Note that Ebert et al. (2007a) suggested that the transition from a pinned to unpinned microstructure should occur at Z~200 μm at our study location, although this boundary is not sharply defined. Apparently, chemical variations between lithologies do not influence the calcite grain size, and, in fact, Ebert et al. (2007a) found no measurable difference in calcite chemistry (e.g. Mn, Mg, Fe, and Sr concentrations) between the Gault and the lower Urgonian at the location of this study. There is, however, substantial local variation in the calcite grain size in samples within the Urgonian, at distances greater than 7 m from the thrust contact and with $Z > 500$ μm, sometimes even when there are no readily apparent second phases (Fig. 6b, $Z = 2000$ μm samples). Finally, samples from the meso-scale shear zones (Fig. 3) within the upper Urgonian have a reduced grain size compared to the host rock (<0.01 m away) (Fig. 4c–d, Fig. 6a–b, samples labeled "loc"), and compared to the grain size predicted by the Zener relation (eq. 1, Fig. 6b).

Second phases

The mineralogy and distribution of second phases varies as a function of primary lithology, and thus also distance to the thrust contact. In the upper and lower Urgonian, second phases are sheet silicates (Fig. 4a–d), with minor quartz (Fig. 5e–f). Second phases may be rare and broadly spaced (e.g., Fig. 4c), or closely spaced and aligned with the primary foliation (e.g. Fig. 4b). Along the boundaries of the meso-scale shear zones, within the upper Urgonian, sheet silicates are often interconnected at the thin-section scale (Fig. 4d). Within the Gault, second phases are predominantly quartz and chlorite (Fig. 5a–d), frequently occurring as fine-grained elongate aggregates, parallel to, and often defining, the primary foliation. The sample closest to the thrust contact (MOG18N1: Fig. 4e, f) is unique in that it contains quartz but no chlorite. In this sample, quartz is either homogeneously mixed with the calcite (Fig. 4f), segregated into bands (Fig. 4e), or present as large porphyroblasts, around which the calcite clearly flows (Fig. 5b). Some layers within this sample are the most quartz rich of any studied (Fig. 4f) whereas other layers contain very little visible quartz (Fig. 4e). In the Gault, coarse-graine d quartz porphyroblasts exhibit undulose extinction (Fig. 5b, d, f), but, in both the Gault and the Urgonian, fine-grained quartz embedded in a calcite matrix frequently shows uniform extinction (Fig. 5a, e). Proximal to the thrust contact, coarse-grained quartz porphyroblasts also appear to be fractured (Fig. 5b).

Crystallographic preferred orientation (CPO)

In all samples, calcite c-axes are preferentially oriented approximately normal to the thrust contact, and a-axes form a girdle in the shear plane (Fig. 4). Samples from the upper and lower Urgonian, with a range of second-phase contents, display back rotation of the calcite c-axes and a-axes with respect to the shear direction (Fig. 4a, b). Such rotations are not seen in finer-

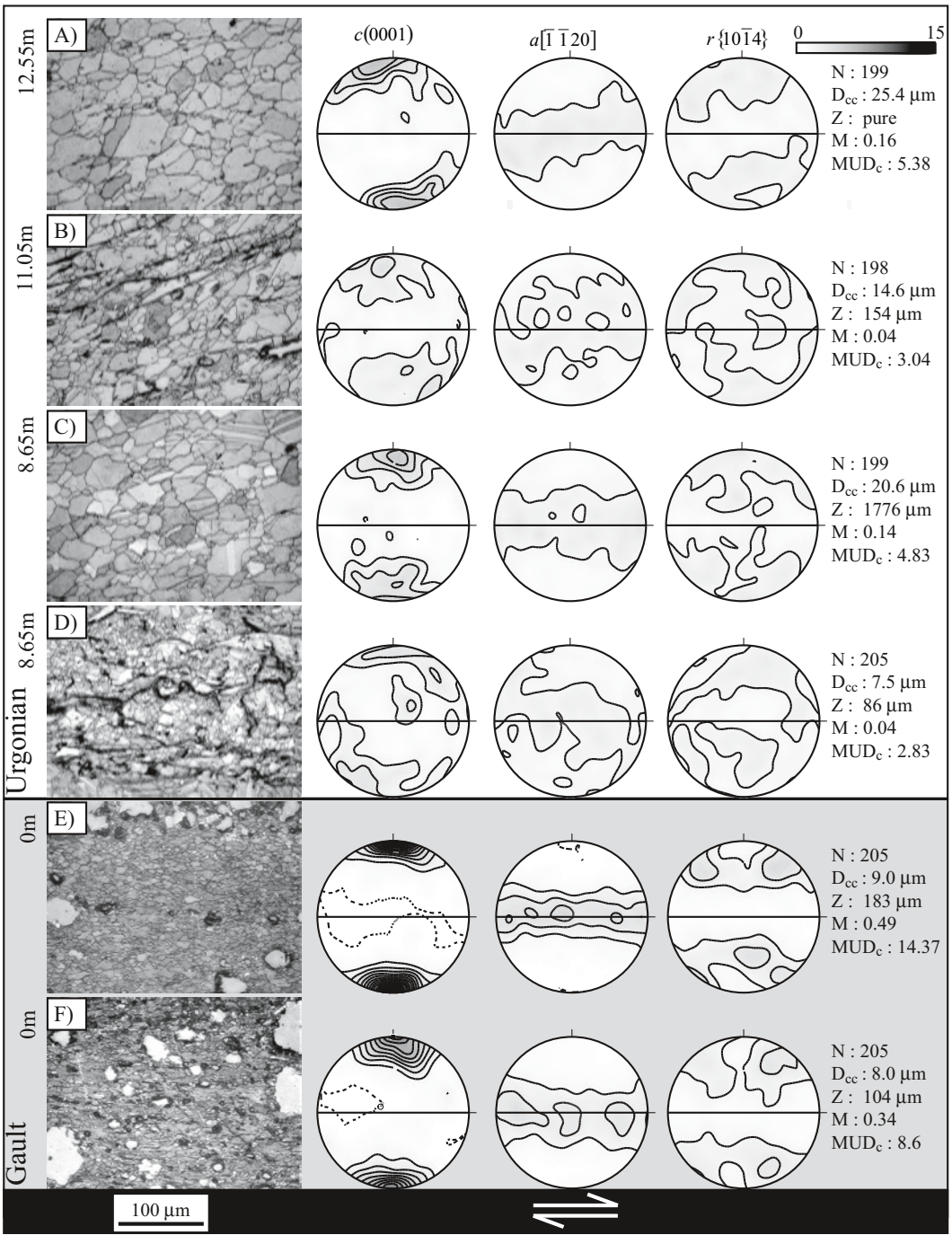

Fig. 4. Microstructures and crystallographic orientations for samples: A) MOUg18N29, B) MOU18N30, C) MOU18N23, D) MOU18N23 "loc", E) and F) MOG18N1 ("loc" refers to samples from the meso-scale shear zones). Pole figures are for c (0001), a [$\bar{1}\,\bar{1}$20], and r {10$\bar{1}$4}. All pole figures are contoured to the same scale (upper right), with maximum multiples of a uniform distribution (MUD) of 15 on a linear grey scale, and a contour interval of 1, using Gaussian smoothing of 8.5º. The horizontal line in each pole figure is parallel to the foliation in the direction of the lineation. N refers to the number of grains (with MAD < 1.3) used to create the pole figure, M is the M-Index (Skemer et al. 2005), and MUD_c is the maximum MUD value on the c-axis pole figure. The distances (in m) refer to estimated distance from the thrust contact, assuming MOG18N1 is on the thrust contact. D_{cc} and Z refer to the mean calcite grain size and the Zener parameter respectively, for the regions analyzed by EBSD (which are shown in the micrographs). A) is the most distal sample from the thrust contact in our data set, and contains no second phases, B) is a sample from near A), however, it contains a large volume of sheet silicates, C) and D) correspond to the box in figure 3d, at the tip of the imbricated layer of Gault within the upper Urgonian. C) Upper Urgonian, approximately 10 mm away from the imbricated Gault layer, containing a very low proportion of second phases whereas D) is from the sheet-silicate rich contact between the imbricated layer of Gault and the upper Urgonian. E) and F) are from the lowermost sample we collected, which is the nearest sample to the thrust contact (see main text). The dominant second phase in this sample is quartz, and the difference between the images is the proportion of quartz.

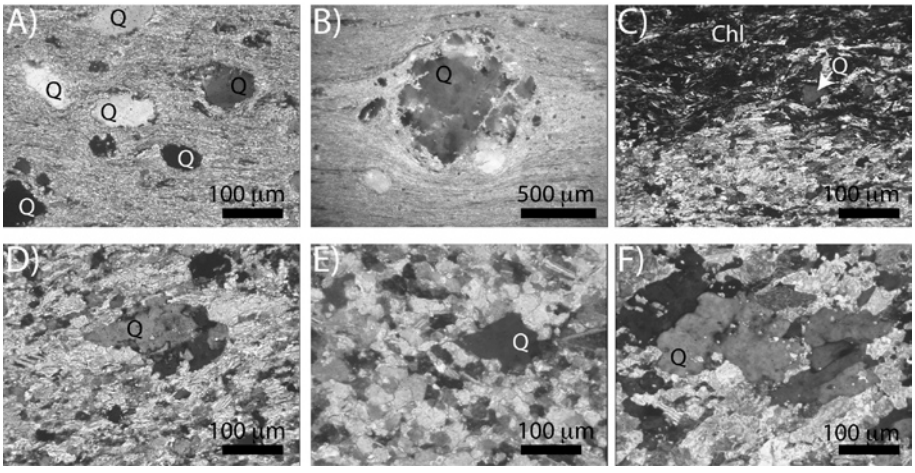

Fig. 5. Transmitted light micrographs of second phases within fine-grained, recrystallized calcite, all shown with a top to the right sense of shear. A-B) Quartz (Q) within sample MOG18N1, from closest to the thrust contact, C) Quartz (Q) and chlorite (Chl) within MOG18N2, 0.25 m above MOG18N1, D) Quartz (Q) within MOG18N4, from 1.05 m above MOG18N1, E) Quartz (Q) within MOU18N14, from 9.50 m above MOG18N1, and F) Quartz (Q) within MOU18N17t from 10.30 m above MOG18N1.

grained calcite near the thrust contact (Fig. 4e, f). The r-poles are moderately inclined to the shear plane, and are sometimes evenly distributed around the c-axes (Fig. 4a, e,f), but in those samples with the strongest preferred orientation (MOG18N1), they form 3 distinct point maxima (Fig. 4e, f). These patterns are similar to those observed by Bestmann et al. (2000) in deformed marbles on Thassos, Greece.

The samples taken from closest to the thrust contact have a stronger preferred orientation, quantified using the M-Index (Figs. 4,7a) compared to all samples from distal to the thrust contact. The degree of preferred orientation is reduced with decreasing calcite grain size (Fig. 7b). However, there are two distinct trends: (a) the samples from <1.05 m above the thrust contact, and (b) all remaining samples. The former gives rise to the increase in CPO intensity proximal to the thrust contact. In samples distal to the thrust contact, the fine-grained regions bounding the meso-scale shear zones have a reduced CPO intensity compared to the coarser-grained calcite which

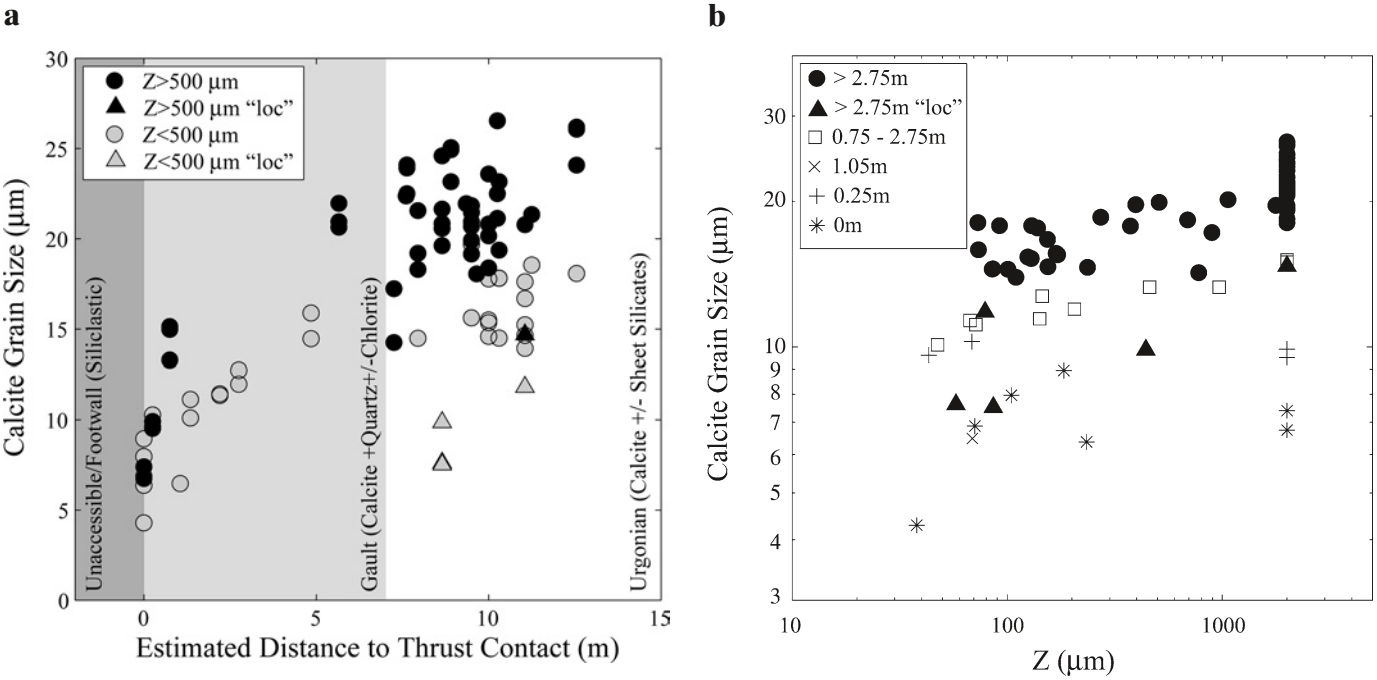

Fig. 6. Variations in grain size as a function of A) estimated distance to the thrust contact, and B) Zener parameter (see section 5.2). The shaded boxes in A) represent the lithologic variations, and the corresponding variations in second phase mineralogy. Samples in A) are distinguished based on Z, using a cutoff of Z = 500 µm, while in B), distances to the thrust contact are highlighted. In both plots, samples obtained from meso-scale shear zones (labeled "loc"), based on field observations, are also highlighted. Z = 2000 µm refers to samples with no second phases visible in the micrographs that were analyzed.

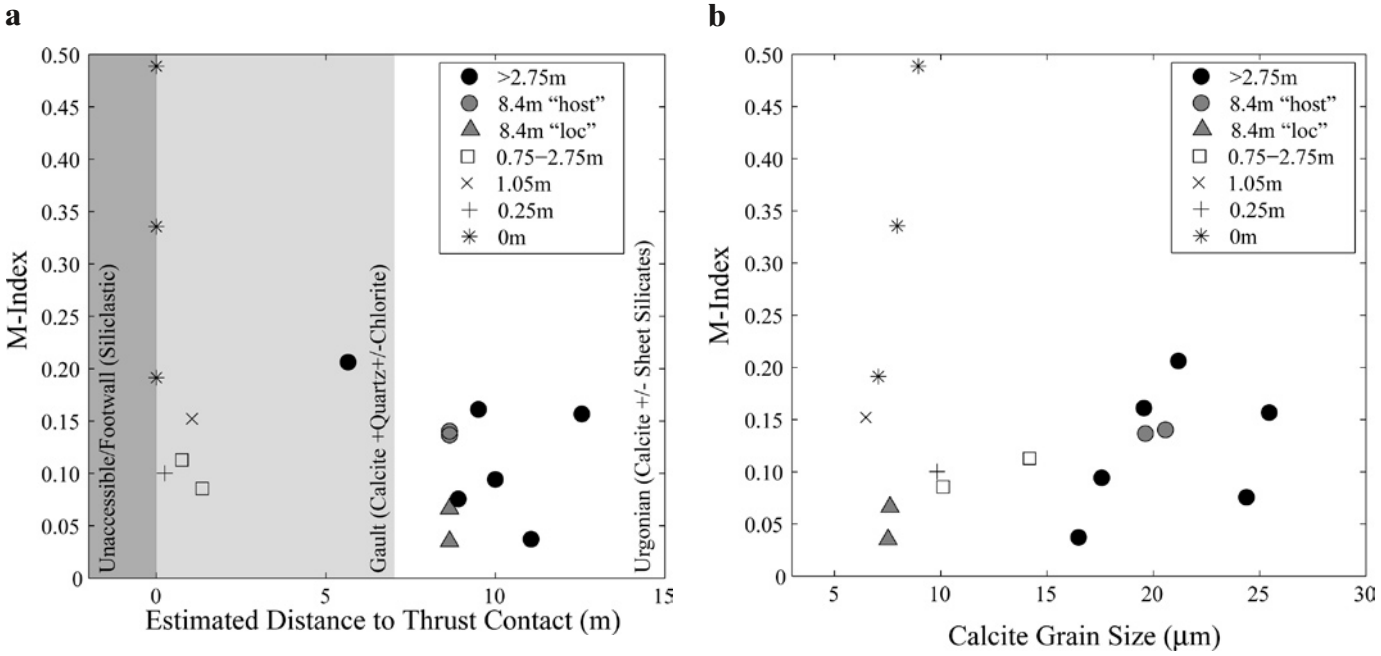

Fig. 7. CPO intensity, quantified using the M-Index (Skemer et al. 2005) as a function of A) estimated distance from the thrust contact, B) calcite grain size. The symbols and grey scale are the same as in figure 6b. As in figures 4 & 6, "loc" refers to samples from the meso-scale shear zones and "host" refers to samples bounding the meso-scale shear zones.

hosts them (Fig. 4c, d). The trend of these features on a plot of M-Index vs. calcite grain size (Fig. 7b) is similar to that for all samples distal to the thrust contact. The sample from closest to the thrust contact, and that from 0.8 m away, also exhibit reduced CPO intensity with decreasing grain size (Fig. 4e, f, 7b). However, despite having grain sizes similar to the fine-grained regions bounding the meso-scale shear zones (Fig. 6b, 7b), these samples have dramatically stronger CPO's (M-Index up to 0.5 compared to <0.05 for the samples from the meso-scale shear zones) (Fig. 4,7). Note that the sample from 0 m (MOG18N1) contains quartz, but no sheet silicates, whereas all other fine-grained samples contain sheet silicates (including chlorite) ± quartz (Fig. 7).

7 Discussion

Deformation mechanisms

At the Saillon cave, at all distances from the thrust contact of the Morcles nappe, matrix-calcite grains have crystallographic preferred orientations (CPO) with c-axis maxima normal to, or slightly antithetically rotated from, the shear plane, and with a-axes distributed within the shear plane. Antithetic rotation of calcite c-axis maxima has also been observed in the Morcles nappe, near Saillon, by Schmid et al. (1981), a pattern that has been attributed to e-twinning, resulting in the alignment of calcite c-axes with the greatest compressive stress (σ_1) (Schmid et al. 1987). Pieri and coworkers (Pieri et al. 2001a; Pieri et al. 2001b) suggested that calcite c-axes progressively rotate during shear deformation, becoming perpendicular to the shear plane with increasing strain. Grains with c-axis maxima normal to the shear plane are preferentially oriented for basal slip (Barber & Wenk 1979; Paterson 1979; De Bresser & Spiers 1993; De Bresser & Spiers 1997; Bestmann et al. 2000; Barber et al. 2007), and the spread of a-axes within the shear plane may be caused by duplex slip in the basal plane (De Bresser & Spiers 1997; Bestmann et al. 2000; Barber et al. 2007). The strong preferred orientation of r-poles (particularly in sample MOG18N1; Fig. 4) can result from simultaneous activation of all three of c-slip, r-slip, and e-twinning as observed in calcite single crystals deformed in both compression and torsion (Wenk et al. 1973; Paterson 1979; De Bresser & Spiers 1990; Wang et al. 1996; Barber et al. 2007). However, we did not quantify the densities of twins, which are not common, particularly in the finest-grained samples (Fig. 4e).

There are two trends of CPO intensity: at a given distance from the thrust contact, M-Indices increase with increasing grain size, particularly in samples distal to the thrust contact and from rocks bearing sheet silicates (Fig. 6). As the distance from the thrust contact varies, the M-Indices, while quite scattered, are roughly constant, except for samples closest to the thrust contact, which exhibit M-Indices between 0.25 and 0.5. The former trend may indicate that a greater proportion of the bulk strain rate was accommodated by grain-boundary sliding in finer grains, that the fine grains, on average, record smaller strains, or that the correlation between total strain and M-Index

Table 2. Grain-size evolution relationships and parameters used to model the Morcles nappe. Labels correspond to those used in the text and in figures. K_g, Q_g, and p are the constants in the normal grain-growth equation, γ is the average grain-boundary energy, c is geometrical constant, and λ is the proportion of mechanical work associated with dislocation creep that is not dissipated, and is thus stored in the microstructure.

Label	Grain Size (Scaling Relationship)	Reference (Scaling Relationship)	Parameters	Reference (Parameters)
AE07	$d_s^{1+p} = \frac{K_g \exp\left(\frac{-Q_g}{RT}\right) p^{-1} c\gamma}{\beta\lambda\sigma\dot{\varepsilon}_{tot}}$	(Austin & Evans 2007)	K_g = 2.5e9 ($\mu m^p\ s^{-1}$)	(Covey-Crump 1997)
	$\beta = \frac{\dot{\varepsilon}_{dis}}{\dot{\varepsilon}_{tot}}$		Q_g = 175 kJ/mol p = 3	
			γ = 1 J m^{-2} c = π λ = 0.1	(Austin & Evans 2007)
S1980	$d_s = B\sigma^{-q}$	(Twiss 1977)	B = $10^{2.63}$ ($\mu m\ MPa^m$) q = 0.9767	(Schmid et al. 1980)
R1995SG	$d_s = B\sigma^{-q}$	(Twiss 1977)	B = $10^{3.31}$ ($\mu m\ MPa^m$) q = 1.14	(Rutter 1995)

differs between coarse and fine-grained rocks. In close proximity to the thrust contact, the carbonates are quartz-bearing; and these, the finest-grained rocks, have the highest CPO intensities. If dislocation activity and CPO intensity are positively correlated (Rutter et al. 1994; Barnhoorn et al. 2004; Warren & Hirth 2006; Mehl & Hirth 2008), deformation within the finest-grained rocks cannot be supposed to have been dominated by diffusion creep, however, we cannot rule out some component of grain-boundary sliding (e.g. Schmid et al. 1987). Measurements of misorientation between neighbouring grains may be used to gain insight into the role of grain-boundary sliding, as well as active slip systems (Bestmann & Prior 2003), but owing to the fine grain size of the Morcles samples, we were unable to perform correlated misorientation measurements.

Pore fluids

To this point, we have neglected the role of pore fluids. As has been well documented by Kirschner et al. (1999), fluid flow was focused along the thrust contact of the Morcles nappe for most of its deformation history. Several authors suggest that water fugacity has little influence on the kinetics of dislocation creep in calcite, both in the laboratory (Rutter 1972; De Bresser et al. 2005) and in natural mylonites (Schenk et al. 2005). But high water pressures will influence pressure solution/fluid-assisted mass-transfer processes (Paterson 1995). At the Saillon cave, the role of fluids likely influenced the formation of the meso-scale shear zones (Fig. 4c, d), which are frequently associated with variably recrystallized veins, have elevated concentrations of sheet silicates, and have the lowest CPO's we observe. Mass transfer in fluids also occurred near the thrust contact, as both quartz and calcite veins are present in the Gault. However, the strong CPO's near the thrust contact at our study location probably indicate that dislocation creep, rather than pressure solution, was the dominant deformation mechanism.

Power dissipation and strain-rate estimates

From grain-size to strain-rate: The paleowattmeter

Grain-size responds to thermodynamic driving forces through the processes of dynamic recrystallization, normal and abnormal grain growth, and chemically induced grain-boundary migration (Urai et al. 1986; Atkinson 1988; Drury et al. 1989; Humphreys & Hatherly 1995; De Bresser et al. 1998; Evans et al. 2001). Many studies suggest that the average grain size at steady state during dynamic recrystallization (d_s) is indirectly related to differential stress (σ) to a power (q) that is of order of unity (Table 2, eq. S1980, R1995SG) (Twiss 1977; Twiss & Sellars 1978; Guillope & Poirier 1979; Karato et al. 1980; Schmid et al. 1980; Gleason et al. 1993; Rutter 1995; Stipp et al. 2001). The mechanism by which steady state is achieved is a topic of some discussion (Guillope & Poirier 1979; Karato et al. 1980; Etheridge & Wilkie 1981; Sakai & Jonas 1984; Urai et

al. 1986; Derby & Ashby 1987; Derby 1991, 1992; Van Der Wal et al. 1993; Rutter 1995; De Bresser et al. 1998; Shimizu 1998; De Bresser et al. 2001; Ter Heege et al. 2002; Hall & Parmentier 2003; Montesi & Hirth 2003; Ter Heege et al. 2005). Some authors have suggested that the stable average grain size represents a balance between the rates of reduction by dynamic recrystallization and of normal grain growth (Derby & Ashby 1987; Derby 1991, 1992; Kameyama et al. 1997; Shimizu 1998; Braun et al. 1999; Shimizu 1999; Hall & Parmentier 2003). De Bresser and coworkers (De Bresser et al. 1998; De Bresser et al. 2001) concluded that this balance might cause the aggregate grain-size to stabilize at a value for which the strain rates owing to dislocation creep and to diffusion creep are equal.

Recently, Austin & Evans (2007) suggested that the grain-size reduction rate during deformation is controlled by the rate that mechanical work is done, and the ability of the rock to either dissipate or store this energy. During deformation, the rate that mechanical work is done per unit volume (power) is the product of stress and strain rate (note that "stress" refers to "differential stress"). The rate of energy input into the system must be balanced by the rate of increase in the internal energy of the system plus the rate that energy is dissipated, which is largely related to heat production and/or other increases in entropy. Because decreased grain size implies increased stored interfacial free energy, Austin & Evans (2007) suggested that the magnitude of $\dot{d}_{reduction}$ is proportional to the rate of mechanical work done on the deforming rock. The existing laboratory data, although sparse (e.g. Karato et al. 1980; Walker et al. 1990) suggest that all of the power input during diffusion creep is completely dissipated, whereas some fraction of the power input during dislocation creep (λ) is stored in the material. Grain-size reduction rates will be enhanced by the increased efficiency of storage, as well as by the relative partitioning of the total strain rate between dislocation creep and diffusion creep. As suggested previously (Kameyama et al. 1997; Braun et al. 1999; Hall & Parmentier 2003), we assume a balance between the rates of static grain growth and reduction by dynamic processes: $\dot{d}_{total} = \dot{d}_{growth} - \dot{d}_{reduction}$, where $\dot{d}_{reduction}$ is explicitly negative. The scaling relationship that results, a paleowattmeter, predicts a stabilized grain size (Table 2, eq. AE07) that is a function of: γ, the specific grain-boundary energy, β, the fraction of the work partitioned into dislocation creep ($\sigma\dot{\varepsilon}_{dis}/\sigma\dot{\varepsilon}_{tot}$); λ, the fraction of that mechanical work stored as internal energy; and K_g, Q_g, p, the constants in the normal grain-growth law ($d^p - d_o^p = K_g \exp\left[\frac{-Q_g}{RT}\right]\Delta t$, Table 2) (Evans et al. 2001; Austin & Evans 2007).

Thus, in this model, recrystallized grain sizes provide information regarding the rate that mechanical work is done during deformation, or the product of stress and strain rate, rather than stress alone. By incorporating the appropriate flow laws into the paleowattmeter (Table 2, eq. AE07), stress and strain rate are simultaneously obtained from the measured grain sizes and measured/estimated thermal conditions during deformation. When published grain-growth laws and dislocation creep flow laws are incorporated into the paleowattmeter, grain sizes obtained in laboratory deformation experiments on calcite, quartz, and olivine are successfully predicted. In the following sections, we will test predictions from the paleowattmeter and paleopiezometers against our observations from the Morcles nappe.

Are microstructures indicative of deformation conditions?

For samples deformed in the laboratory at high temperatures, it is sometimes difficult to distinguish microstructures formed during static grain growth from those formed during deformation. So, before applying the paleowattmeter and paleopiezometers to the natural microstructure data, we consider the possibility that grain sizes have been influenced by annealing and grain growth after deformation. Fine recrystallized grains are universally present, particularly in the coarsest-grained samples (Fig. 4a, c). Further, Herwegh and coworkers (Herwegh & Berger 2003; Herwegh et al. 2005; Ebert et al. 2007b) argue that the grain size of rocks with varying second-phase content, if annealed at similar conditions, will exhibit a positive slope in $d_s - Z$ space (where d_s is the stable grain size), for all Z values, because grains will grow until they interact with a pinning phase. The average grain size of our samples and those of Ebert et al. (2007a) from this study location, do not vary with Z when $Z > 500$ μm (Fig. 6b). However, we cannot rule out the possibility that some coarsening related to annealing occurred; thus, incomplete coarsening might be responsible for some of the scatter observed in calcite grain size for samples with no visible second phases (Fig. 6b, $Z = 2000$ μm). Such coarsening, if present, did not, however, proceed to the fully pinned state. The strong correlation between grain size and distance to the thrust contact also indicates that there has not been extensive annealing.

An additional possibility is that the matrix grain size has not reached a steady state, due to incomplete recrystallization. However, two lines of evidence suggest that the measured recrystallized grain sizes are representative of the deformation conditions. First, where calcite veins are present they exhibit incomplete recrystallization, with recrystallized grains having the same grain size as the matrix calcite (Fig. 5). Herwegh et al. (2005) made similar observations on the Doldenhorn nappe and Gellihorn and Wildhorn nappes, and drew the same conclusion as we do here: measured grain sizes are indicative of deformation conditions. Further, in the fine-grained, micritic limestones of the Doldenhorn nappe (the eastern extension of the Morcles nappe) grain growth seems to have occurred in the matrix as grains in nearby veins were reduced with both reaching similar final grain sizes (Herwegh et al., 2005). The suggestion is that, not only are microstructures indicative of the deformation conditions, but also that these microstructures result from competing grain-growth and grain-size reduction processes; an inherent assumption of the paleowattmeter. Second at all distances from the thrust contact, the primary folia-

Table 3. Calcite flow laws and parameters used to model the Morcles nappe. Equation labels correspond to those used in the text and in figures.

Label	Flow Law	Type	Parameters	Reference
Rp	$\dot{\varepsilon}_p = A_p \sigma^2 \exp\left(\frac{\sigma}{\sigma_p}\right) \exp\left(-\frac{Q_p}{RT}\right)$	Dislocation Creep	A_p = 270.4 (MPa^{-2} s^{-1})	(Renner et al. 2002)
	$\sigma_p = \left[\Sigma_{p,o} + K_p d^{-m_p}\right]\left[Tm - T\right]$	(Peierls Law)	Q_p = 200 kJ/mol m_p = 0.5 K_p = 115 (MPa μm^{mp} kK^{-1}) $\Sigma_{p,o}$ = 7.8 (MPa kK^{-1}) Tm = 1600 (K)	
Sdis	$\dot{\varepsilon}_{dis} = A_{dis} \sigma^{n_{dis}} \exp\left(-\frac{Q_{dis}}{RT}\right)$	Dislocation Creep	A_{dis} = 2511.9 (MPa^{-ndis} s^{-1})	(Schmid et al. 1977)
		(Power Law)	n_{dis} = 4.7 Q_{dis} = 297 kJ/mol	
Sdif	$\dot{\varepsilon}_{dif} = A_{dif} \sigma^{n_{dif}} d^{-m_{dif}} \exp\left(-\frac{Q_{dif}}{RT}\right)$	Diffusion Creep	A_{difs} = 19952.6 (MPa^{-ndifs} μm^{-mdifs} s^{-1}) n_{difs} = 1.66 m_{difs} = –2.5 Q_{difs} = 209 kJ/mol	(Schmid et al. 1977)
Wdif	$\dot{\varepsilon}_{dif} = A_{dif} \sigma^{n_{dif}} d^{-m_{dif}} \exp\left(-\frac{Q_{dif}}{RT}\right)$	Diffusion Creep	A_{difw} = 79432.8 (MPa^{-ndifw} μm^{-mdifw} s^{-1}) n_{difw} = 1.7 m_{difw} = –1.9 Q_{difw} = 190 kJ/mol	(Walker et al. 1990)
Hdif	$\dot{\varepsilon}_{dif} = A_{dif} \sigma^{n_{dif}} d^{-m_{dif}} \exp\left(-\frac{Q_{dif}}{RT}\right)$	Diffusion Creep	A_{difh} = 4.3e7 (MPa^{-ndifh} μm^{-mdifh} s^{-1}) n_{difh} = 1.1 m_{difh} = –3.3 Q_{difh} = 200 kJ/mol	(Herwegh et al. 2003)

tion is approximately parallel to the shear zone, consistent with the observations of Ramsay (1981), Schmid et al. (1981), and Ebert et al. (2007a) that all of the limestones in the inverted limb of the Morcles nappe are highly sheared, frequently exhibiting axial ratios of >90:1. Based on laboratory studies (Pieri et al. 2001a; Pieri et al. 2001b; Barnhoorn et al. 2004), we expect to find complete recrystallization at shear strains greater than ~10, well below the minimum strains in all of our samples. From these constraints, we infer that variations in calcite grain size correspond to variations in the conditions of deformation.

Stresses and strain rates along the inverted limb of the Morcles nappe

We applied the paleowattmeter and paleopiezometers (Eqs. AE07, S1980, R1995SG, Table 2) to the data from samples with $Z > 500$ μm from the upper Urgonian at various positions along the Morcles nappe (Ebert et al. 2007a) (Figs. 2 and 8a). We limit our analysis to flow laws for fine-grained carbonates (Schmid et al. 1977; Walker et al. 1990; Renner et al. 2002; Herwegh et al. 2003) (Table 3), as these are most applicable to the microstructures observed in the Morcles nappe. Note that the parameters in these flow laws were obtained from experiments run to relatively low strains in triaxial compression: we will address the role of strain softening, as observed by Barnhoorn et al. (2004) during high-strain torsion experiments on coarse-grained Carrara marble, in the next section.

If grain-growth parameters from Covey-Crump (1997) and dislocation creep flow laws for synthetic marbles (Renner et al. 2002) (Table 3, Rp) or for Solnhofen limestone (Schmid et al. 1977) (Table 3, Sdis) are used, equation AE07 predicts values of $\sigma\dot{\varepsilon}_{dis}$ consistent with strain rates from dislocation creep between 10^{-10} and 10^{-12} s^{-1} (Fig. 8a, b). The total strain rate may be estimated by using diffusion creep and dislocation creep laws, and the assumption that $\dot{\varepsilon}_{tot} = \dot{\varepsilon}_{dif} + \dot{\varepsilon}_{dis}$ (Ter Heege et al. 2004; Herwegh et al. 2005). For the dislocation and diffusion

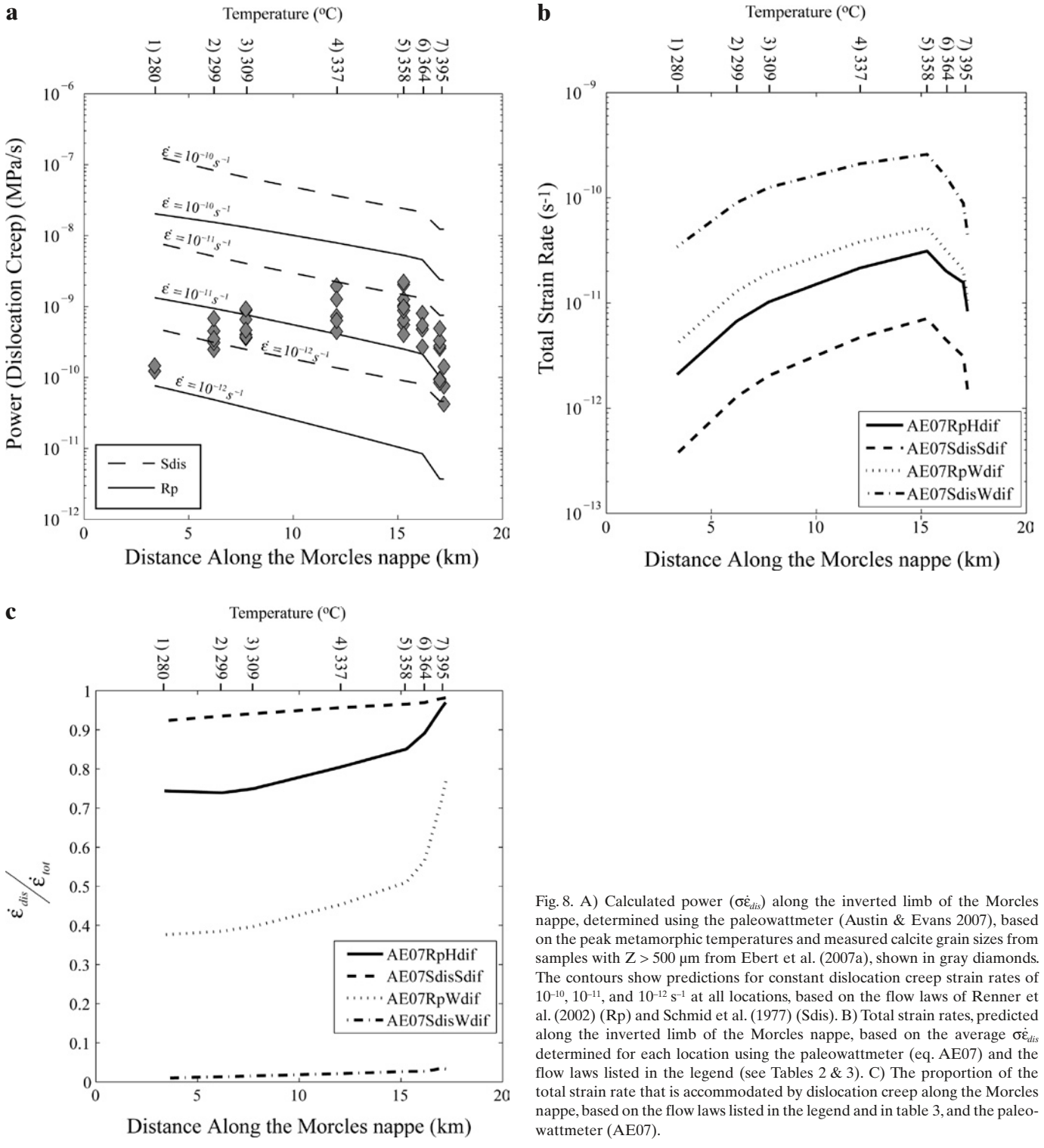

Fig. 8. A) Calculated power ($\sigma\dot{\varepsilon}_{dis}$) along the inverted limb of the Morcles nappe, determined using the paleowattmeter (Austin & Evans 2007), based on the peak metamorphic temperatures and measured calcite grain sizes from samples with Z > 500 μm from Ebert et al. (2007a), shown in gray diamonds. The contours show predictions for constant dislocation creep strain rates of 10^{-10}, 10^{-11}, and 10^{-12} s^{-1} at all locations, based on the flow laws of Renner et al. (2002) (Rp) and Schmid et al. (1977) (Sdis). B) Total strain rates, predicted along the inverted limb of the Morcles nappe, based on the average $\sigma\dot{\varepsilon}_{dis}$ determined for each location using the paleowattmeter (eq. AE07) and the flow laws listed in the legend (see Tables 2 & 3). C) The proportion of the total strain rate that is accommodated by dislocation creep along the Morcles nappe, based on the flow laws listed in the legend and in table 3, and the paleowattmeter (AE07).

creep flow laws in table 3, the strain-rate profiles in figure 8b are predicted for the length of the nappe. The predicted strain rates are slightly faster (~10^{-11} s^{-1}), but still roughly consistent with values constrained by the field structural data (Ebert et al., 2007a; 10^{-11} to 10^{-13} s^{-1}). The dislocation creep flow laws of Renner et al. (2002) (Rp) and Schmid et al. (1977) (Sdis), when coupled with a diffusion creep flow law for the same material, Herwegh et al. (2003) (Hdif) and Schmid et al. (1977)

(Sdif), respectively, both suggest that the total strain rate is dominated by dislocation creep (Fig. 8c), consistent with the CPO observations of Ebert et al. (2007a), particularly in the higher temperature portions of the shear zone. But, if the diffusion creep parameters from Walker et al. (1990) (Wdif) are used with either dislocation creep flow law, diffusion creep is predicted to dominate.

The paleowattmeter suggests that the power increased from the root zone, reached a peak at distances of 12–14 km from the fold hinge, and then progressively decreased towards the hinge (Fig. 8b). Field relations indicate that the total displacement accommodated across the inverted limb of the Morcles nappe decreased progressively from ~12km at the Saillon cave to 0 km at the fold hinge, and that the shear zone narrows. Thus, strain rates are believed to remain roughly constant along the shear zone (Ebert et al. 2007a). But, without denser sampling along the shear zone, it is difficult to be more precise.

At the lower temperatures estimated near the toe of the nappe, it may be that deformation occurred, at least in part, by other mechanical processes, e.g., granular flow, fracture, or pressure solution. None of these processes are included in the paleowattmeter or the composite flow law that we have considered, so their presence might be responsible for the apparent decrease in power and strain rate as recorded in the grain sizes. CPO intensities also decrease towards the frontal portions of the nappe (Ebert et al. 2007a), as might be consistent with partitioning of strain into cataclastic mechanisms; however, this decrease might also be caused by variations in total strain. Also note that, at the temperatures and grain sizes investigated in the Morcles nappe, the paleopiezometer calibrations of Schmid et al. (1980) and Rutter (1995) bound the predictions of the paleowattmeter, when the dislocation creep flow law of Renner et al. (2002) (Rp) is used. Variations in the stress predicted by the several piezometers may arise owing to differences in technique used to the measure grain size (Rutter 1995; De Bresser 2002). In this study, we simply use the reported grain-size values, without attempting to resolve differences in techniques.

Stress and/or strain rate variations normal to the thrust contact

At the Saillon cave, in carbonate samples where grain-boundary pinning is unlikely ($Z > 500$ μm), the paleowattmeter suggests that significantly more power was dissipated near the thrust contact (Fig. 9a). The fine-grained samples nearer to the thrust contact also have the strongest CPO's of any samples we investigated (Fig. 4e, f, 7a), and, on average, the highest quartz contents (Fig. 4–6). The reduced grain size, and increased power closest to the thrust contact can be explained in two ways: 1) there may have been temporal and spatial variations in stress, or 2) the limestones nearest the thrust contact may have strain weakened, resulting in progressive strain localization and increased strain rates at constant stress.

Using any of the flow laws (Table 3) and the paleowattmeter, we predict both elevated stresses and strain rates in the finest-grained rocks closest to the thrust contact (Figs. 9b, c). If this scenario is correct, stress must have varied temporally, as mechanical considerations preclude contemporaneous stress variations normal to the thrust contact in a simple thrusting geometry. Stress variations may have occurred if there were significant variations in the orientation of the lithological contact between the inverted limb of the Morcles nappe and the Triassic cover of the Aiguille Rouge massif, however, in outcrop we see no evidences of any deviation from a simple, relatively flat, thrust-fault geometry.

As with the variations along the inverted limb of the Morcles nappe, the stresses along a profile normal to the thrust contact predicted by the paleowattmeter and the dislocation creep flow law of Renner et al. (2002) (Rp) are bound by the predictions of the paleopiezometers of Schmid et al. (1980) (S1980) and Rutter (1995) (subgrain: R1995SG). If, instead, the paleowattmeter, and the dislocation creep flow law from Schmid et al. (1977) (Sdis) are used, stresses are approximately a factor of 2–3 higher. Rutter's grain boundary migration piezometer (Rutter 1995) (not shown) predicts stresses of ~180 MPa in the upper Urgonian, and stresses >450 MPa closest to the thrust contact, in the Gault.

The limestones nearest the thrust contact are quartz-rich. Experimental studies have shown that the addition of as little as 5 vol% uniformly dispersed quartz to fine-grained calcite aggregates increases the strength of the material (Dresen et al. 1998; Rybacki et al. 2003; Xiao & Evans 2003; Renner et al. 2007). However, it is difficult to envision this strength variation resulting in contemporaneous stress variations across the shear zone, when quartz-rich limestones (Gault) are juxtaposed with pure limestones (Urgonian).

Temporal variations in loading geometry are mechanically admissible. An alternative explanation might be that stresses increased as temperature decreased (Kirschner et al. 1996). Ebert et al. (2007a) have suggested that progressive localization occurred under retrograde conditions. However, again considering the juxtaposition of relatively pure and impure limestones, we would expect elevated stresses to be recorded in all microstructures, particularly in the pure limestones of the Urgonian. Thus stress variations of a factor of ~3 recorded over a spatial scale of less than 15 m seem unlikely.

We now consider a second, more plausible, scenario: the increase in power closest to the thrust contact resulted from strain weakening of the material, leading to an increase in strain rate at constant stress. This hypothesis is consistent with theoretical and experimental considerations of strain localization (Hobbs et al., 1990; Rutter, 1999). If we assume that stresses were constant in sections normal to the thrust contact, then a >10-fold enhancement in strain rate in the rocks closest to the thrust contact would be required to explain the power predictions from the paleowattmeter (Fig. 9a), regardless of which dislocation creep flow law is chosen. For example, if the stress was 35 MPa throughout the shear zone, the paleowatt-

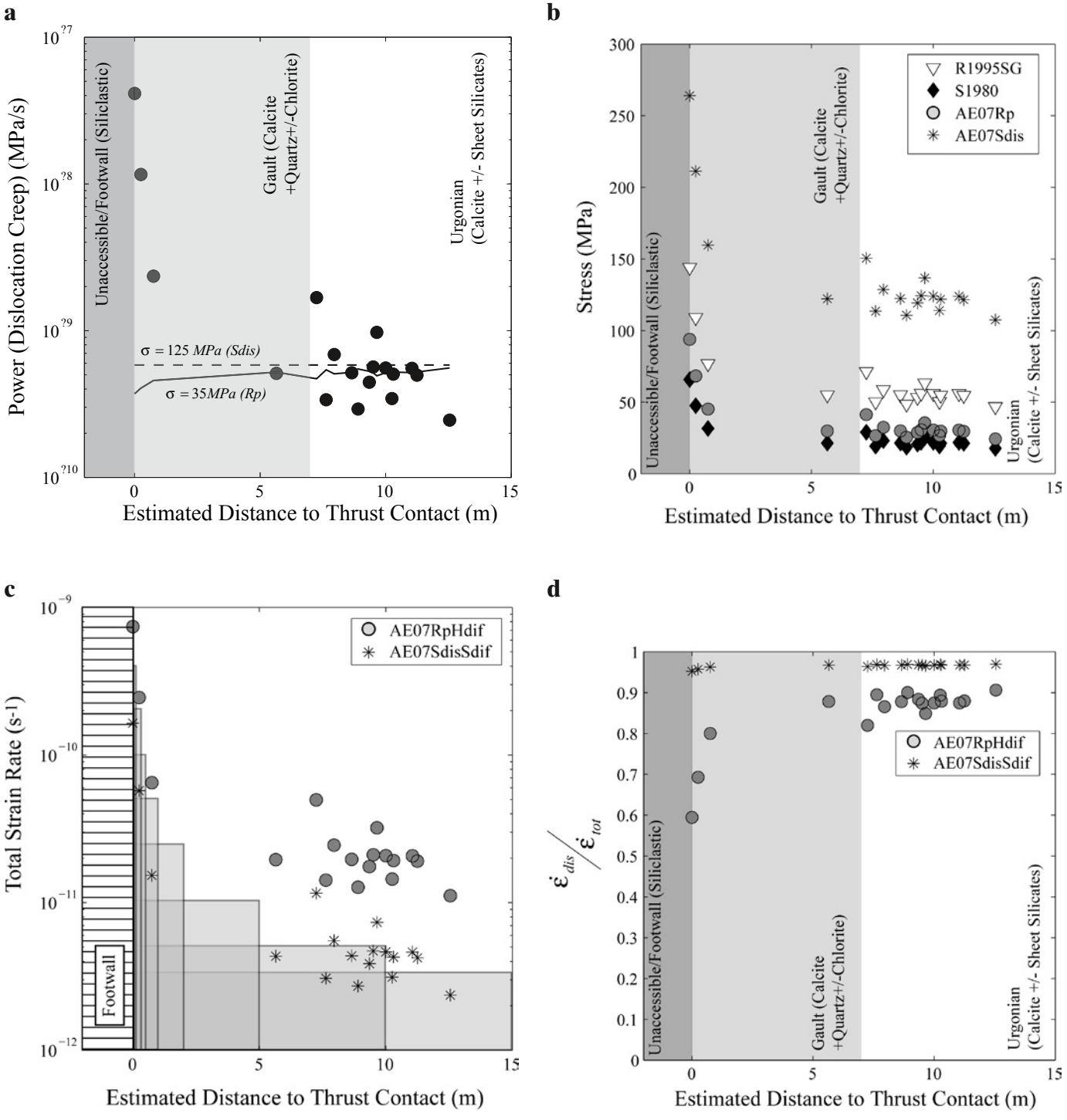

Fig. 9. A) Variations in the power associated with dislocation creep ($\sigma\dot{\varepsilon}_{dis}$) perpendicular to the thrust contact, based on predictions from the paleowattmeter (AE07) and the measured calcite grain sizes reported in table 1. The contours show the predictions for constant differential stress (as labeled) normal to thrust contact using the dislocation creep flow laws of Renner et al. (2002) (Rp) and Schmid et al. (1977) (Sdis). B) Differential stress variations normal to the thrust contact, based on the predictions of the relationships in table 2 (AE07, S1980, R1995SG). Stresses were determined from the paleowattmeter (AE07) using the dislocation creep flow laws of Renner et al. (2002) (Rp) and Schmid et al. (1977) (Sdis) and from the paleopiezometers (S1980, R1995SG). The only plausible mechanical explanation for this scenario is a temporal evolution in stress (though see text for a further discussion). C) Strain rate variations normal to the thrust contact based on the paleowattmeter (AE07) and a composite flow law using either the parameters from Renner et al. (2002) (Rp) & Herwegh et al. (2003) (Hdif) or Schmid et al. (1977) (Sdis & Sdif). The grey boxes correspond to the shear-zone thickness required, for the corresponding strain rate, to accommodate the average regional displacement rate while the Morcles nappe was actively deforming. D) The proportion of the total strain rate that is accommodated by dislocation creep perpendicular to the contact between the inverted limb of the Morcles nappe and the Triassic cover of the Aiguille Rouge massif, based on the flow laws listed in the legend and in table 3. All calculations were performed assuming a peak metamorphic temperature of 358 °C.

meter predicts strain rates nearly equivalent to those labelled AE07RpHdif in figure 9c, whereas if the stress was 125 MPa, the predicted strain-rate distribution is closer to that labelled AE07SdisSdif.

Multiphase materials might weaken, particularly if the stronger phase reorganizes into a foliation plane (Handy 1990, 1994; Ji et al. 2004; Barnhoorn et al. 2005), or if a strong CPO is formed (Pieri et al. 2001a; Pieri et al. 2001b; Barnhoorn et al. 2004). In those studies on coarse-grained marbles, a 20–25% weakening was observed at constant strain rate, equivalent to a 3–4-fold enhancement of strain rate under constant stress conditions. The rocks in the Morcles nappe have undergone at least 5–10 times more total strain than even the highest-strain experiments in the studies discussed above, and considering the strength of the CPO's in the samples from closest to the thrust contact of the Morcles nappe, a 10-fold strain-rate enhancement may not be unreasonable (Fig. 7a).

Based on the assumption that strong CPO's indicate deformation was dominated by dislocation creep, weakening cannot have been related to a switch in deformation mechanism from dislocation creep to diffusion creep, associated with grain-size reduction. Both sets of flow laws we investigated also suggest that deformation was dominated by dislocation creep (Fig. 9d) even withstanding any assumptions regarding geometric weakening.

Estimating the temporal and spatial evolution of strain

If the shear zone initially had a thickness of 50 m, and was deforming at a strain rate of 10^{-12} s^{-1} (Ebert et al. 2007a), then the regional displacement rate was ~1.6 mm/yr. This average slip rate could accommodate the ~12 km of offset estimated for the Saillon cave (Ebert et al. 2007a) in the ~8 ma that the inverted limb of the Morcles nappe was actively deforming (Loup 1992; Kirschner et al. 1999). Using the paleowattmeter (Austin & Evans 2007), the dislocation creep flow laws of Renner et al. (2002) (Rp) or Schmid et al. (1977) (Sdis), and the diffusion creep flow laws of Herwegh et al. (2003) (Hdif) or Schmid et al. (1977) (Sdif), the strain rates calculated at each distance from the contact between the inverted limb of the Morcles nappe and the Triassic cover of the Aiguille Rouge massif are consistent with the shear-zone thicknesses required to accommodate the regional displacement rate (Fig. 9c). Assuming the regional displacement rates remained approximately constant during thrusting of the Morcles nappe, this suggests that, in agreement with Ramsay et al. (1983), with progressive thrusting, the active zone of intense shear became narrower, and the microstructure is thus recording the peak strain rates at a given position. If temperatures were lower than the peak metamorphic temperatures, lower strain rates would be predicted from the observed microstructure, thus requiring a broader shear zone to accommodate the same displacement rate. For example, at 308 °C the AE07RpHdif composite flow law predicts similar total strain rates to the AE07SdisSdif composite flow law at 358 °C (Fig. 9c).

Several key uncertainties will influence this analysis. First, as discussed above, there is significant uncertainty in the absolute values of the temperature estimates for each location, although the relative temperatures appear to be robust (Ebert et al. 2007a). Secondly, the regional displacement rate might have varied over time. Lastly, we do not, at present, have good constraints on the total displacement accommodated by the meso-scale shear zones, so we cannot quantify the fraction of the regional displacement rate that these features accommodated. Despite these uncertainties, the agreement between the predicted distribution of strain rate and that required to explain the tectonic environment during nappe emplacement is striking.

Implications for the emplacement of the Helvetic nappes

Reduced grain sizes are frequently observed in association with mylonite shear zones, including in deformed limestones throughout the Helvetic zone. For example in the Doldenhorn nappe and Glarus thrust, Herwegh & Pfiffner (2005) and Ebert et al. (2007b), respectively, documented similar grain-size profiles with decreasing distance to the thrust contact as we have observed in the Morcles nappe. However, unlike in the present study on the Morcles nappe where the strongest CPO intensities were found in the finest-grained limestone mylonites closest to the thrust contact, these previous studies documented reduced CPO intensities in the finest-grained rocks closest to the thrust contact in both the Doldenhorn nappe (Herwegh & Pfiffner 2005) and Glarus thrust (Ebert et al. 2007b). Earlier workers have made similar observations on the Glarus thrust (Schmid et al. 1977; Pfiffner 1982). All of these previous studies attributed the correlation between fine grain sizes and weak CPO intensities to a transition from dislocation creep dominated deformation at coarse grain sizes to grain size sensitive diffusion creep and/or dislocation creep accommodated grain boundary sliding at finer grain sizes. However, both along the Glarus thrust (Ebert et al. 2007b) and in the Gellihorn nappe (Herwegh & Kunze 2002; Herwegh et al. 2005) fine-grained layers with a strong CPO are found juxtaposed with layers having a similarly fine grain size and a weak CPO. More detailed work is necessary to quantitatively relate CPO intensity with deformation mechanisms and mechanical properties; however, these observations suggest that the mechanical evolution of limestone mylonites may have differed between the different Helvetic nappes, possibly resulting in variations in the temporal evolution of the distribution of strain. If so, the mechanical history of the various Helvetic nappes may have been markedly different, thus influencing the overall evolution of the Helvetic zone, although much more work is required to quantify this statement.

8 Conclusions

In samples where there is no evidence of second-phases influencing the calcite grain size ($Z > 500$ μm), there is a signifi-

cant reduction in calcite grain size, and concomitant increase in CPO intensity with decreasing distance to the thrust contact. When second phases are present ($Z < 500$ μm), these poison calcite grain-growth, resulting in a finer calcite grain size.

We have used the paleowattmeter to estimate strain rates within the inverted limb of the Morcles nappe. When the paleowattmeter is applied to samples with $Z > 500$ μm collected previously from several locations along the nappe, the strain-rates predicted using published flow laws are consistent with estimates based on geologic observations. If the grain size along a transect perpendicular to the thrust contact is interpreted by the paleopiezometers, stresses are predicted to vary, and to be higher closer to the thrust contact. However, due to mechanical considerations, this scenario seems unlikely. If stresses are assumed to be constant along the transect, the paleowattmeter suggests material weakening, which is consistent with theoretical considerations pertaining to strain localization. Such weakening might be associated with the formation of CPO and a strong foliation, both of which are observed close to the thrust contact. Further, our CPO observations suggest that deformation was accommodated by dislocation creep, despite the fine grain size.

To fully understand strain localization in multiphase rocks, more work needs be done investigating the coupling between CPO formation, grain-size evolution, foliation development, and rheological properties. Despite these uncertainties, the deformation conditions predicted using the paleowattmeter and calcite flow laws are in good agreement with both microstructural and regional scale observations along the Morcles nappe.

Acknowledgements

We would like to thank Greg Hirth, Louie Kerr, Luc Mehl, and Jessica Warren for assisting us with the EBSD system at WHOI. Dirk Rieke-Zapp was extremely helpful in the field, and Uli Mok provided assistance with image analysis. Reviews by Luigi Burlini, Stefan Schmid, and an anonymous reviewer greatly improved this manuscript, as did discussions with Clark Burchfiel and Peter Kelemen. The thin section lab at the University of Bern kindly prepared the thin sections. This work was supported by NSF grants EAR0510412 and OCE-0452787 (BE), GSA student research grant 7586-04 (NA), SNF grants 21-66889.01 and 200020-103720 (MH), and the MIT Student Research Fund (NA).

REFERENCES

Atkinson, H. 1988: Theories of normal grain growth in pure single phase systems. Acta Metallurgica 36, 469–491.

Austin, N. & Evans, B. 2007: Paleowattmeters: A scaling relation for dynamically recrystallized grain size. Geology 35(4), 343–346.

Badoux, H. 1972: Tectonique de la nappe de Morcles entre Rhône et Lizerne: Matériaux pour la Carte Géologique de la Suisse. Nouvelle Série 143, 1–74.

Barber, D. & Wenk, H. 1979: Deformation twinning in calcite, dolomite, and other rhombohedral carbonates. Physics and Chemistry of Minerals 5(2), 141–165.

Barber, D., Wenk, H., Gomez-Barreiro, J., Rybacki, E. & Dresen, G. 2007: Basal slip and texture development in calcite: new results from torsion experiments. Physics and Chemistry of Minerals 34(2), 73–84.

Barnhoorn, A., Bystricky, M., Burlini, L. & Kunze, K. 2004: The Role of Recrystallization on the Deformation Behaviour of Calcite Rocks: High Strain Torsion Experiments on Carrara Marble. Journal of Structural Geology 26, 885–903.

Barnhoorn, A., Bystricky, M., Kunze, K., Burlini, L.& Burg, J. 2005: Strain localization in bimineralic rocks: Experimental deformation of synthetic calcite–anhydrite aggregates. Earth and Planetary Science Letters 240(3–4), 748–763.

Bestmann, M., Kunze, K. & Matthews, A. 2000: Evolution of a calcite marble shear zone complex on Thassos Island, Greece: microstructural and textural fabrics and their kinematic significance. Journal of Structural Geology 22(11–12), 1789–1807.

Bestmann, M. & Prior, D. 2003: Intragranular dynamic recrystallization in naturally deformed calcite marble: diffusion accommodated grain boundary sliding as a result of subgrain rotation recrystallization. Journal of Structural Geology 25(10), 1597–1613.

Boullier, A. & Quenardel, J. 1981: The Caledonides of northern Norway: relation between preferred orientation of quartz lattice, strain and translation of the nappes. Geological Society London Special Publications 9(1), 185–195.

Braun, J., Chéry, J., Poliakov, A., Mainprice, D., Vauchez, A., Tomassi, A. & Daignières, M. 1999: A simple parametrization of strain localization in the ductile regime due to grain size reduction: A case study for olivine. Journal of Geophysical Research 104(B11), 25167–25182.

Bucher, S., Schmid, S., Bousquet, R. & Fugenschuh, B. 2003: Late-stage deformation in a collisional orogen (Western Alps): nappe refolding, backthrusting or normal faulting? Terra Nova 15(2), 109–117.

Burg, J. 1999: Ductile structures and instabilities: their implication for Variscan tectonics in the Ardennes. Tectonophysics 309(1), 1–25.

Burkhard, M. 1988: L'Helvétique de la bordure occidentale du massif de l'Aar (évolution tectonique et métamorphique). Eclogae Geologicae Helvetiae 81(1), 63–114.

Burkhard, M. & Kerrich, R. 1988: Fluid regimes in the deformation of the Helvetic nappes, Switzerland, as inferred from stable isotope data. Contributions to Mineralogy and Petrology 99(4), 416–429.

Burkhard, M. & Goy-Eggenberger, D. 2001: Near vertical iso-illite-crystallinity surfaces crosscut the recumbent fold structure of the Morcles nappe, Swiss Alps. Clay Minerals 36(2), 159–170.

Burlini, L. & Bruhn, D. 2005: High-strain zones: laboratory perspectives on strain softening during ductile deformation. Geological Society London Special Publications 245(1), 1.

Covey-Crump, S. 1997: The normal grain growth behavior of nominally pure calcitic aggregates. Contributions to Mineralogy and Petrology 129(2), 239–254.

Coward, M. & Dietrich, D. 1989: Alpine tectonics – an overview. Geological Society London Special Publications 45(1), 1–29.

Crespo-Blanc, A., Masson, H., Sharp, Z., Cosca, M. & Hunziker, J. 1995: A stable and 40 Ar/39 Ar isotope study of a major thrust in the Helvetic nappes (Swiss Alps); evidence for fluid flow and constraints on nappe kinematics. Bulletin of the Geological Society of America 107(10), 1129–1144.

De Bresser, J. & Spiers, C. 1990: High-temperature deformation of calcite single crystals by r+ and f+ slip. Geological Society London Special Publications 54(1), 285–298.

De Bresser, J. & Spiers, C. 1993: Slip systems in calcite single crystals deformed at 300–800 C. Journal of Geophysical Research 98(B4), 6397–6409.

De Bresser, J. & Spiers, C. 1997: Strength characteristics of the r, f, and c slip systems in calcite. Tectonophysics 272(1), 1–23.

De Bresser, J., Peach, C., Reijs, J. & Spiers, C. 1998: On dynamic recrystallization during solid state flow: Effects of stress and temperature. Geophysical Research Letters 25(18), 3457–3460.

De Bresser, J., Ter Heege, J. & Spiers, C. 2001: Grain size reduction by dynamic recrystallization: can it result in major rheological weakening? International Journal of Earth Sciences 90(1), 28–45.

De Bresser, J. 2002: On the mechanism of dislocation creep of calcite at high temperature: inferences from experimentally measured pressure sensitivity and strain rate sensitivity of flow stress. Journal of Geophysical Research 107(B12), doi:10.1029/2002JB001812.
De Bresser, J., Urai, J. & Olgaard, D. 2005: Effect of water on the strength and microstructure of Carrara marble axially compressed at high temperature. Journal of Structural Geology 27(2), 265–281.
Derby, B. & Ashby, M. 1987: On Dynamic Recrystallization. Scripta Metallurgica et Materialia 21(6), 879–884.
Derby, B. 1991: The Dependence of Grain Size on Stress During Dynamic Recrystallization. Acta Metallurgia et Materialia 39(5), 955–962.
Derby, B. 1992: Dynamic recrystallisation. The steady state grain size. Scripta Metallurgica et Materialia 27(11), 1581–1586.
Dietrich, D. & Song, H. 1984: Calcite fabrics in a natural shear environment, the Helvetic nappes of western Switzerland. Journal of Structural Geology 6(1–2), 19–32.
Dietrich, D. 1986: Calcite fabrics around folds as indicators of deformation history. Journal of Structural Geology 8(6), 655–668.
Dietrich, D. & Durney, D. 1986: Change of direction of overthrust shear in the Helvetic nappes of western Switzerland. Journal of Structural Geology 8(3–4), 389–398.
Dietrich, D. 1989: Fold axis parallel extension in an arcuate fold and thrust belt: the case of the Helvetic nappes. Tectonophysics 170, 183–212.
Dietrich, D. & Casey, M. 1989: A new tectonic model for the Helvetic nappes. Geological Society London Special Publications 45(1), 47–63.
Dresen, G., Evans, B. & Olgaard, D. 1998: Effect of quartz inclusions on plastic flow in marble. Geophysical Research Letters 25(8), 1245–1248.
Drury, M., Humphreys, F. & White, S. 1989: Effect of dynamic recrystallization on the importance of grain-boundary sliding during creep. Journal of Materials Science 24(1), 154–162.
Ebert, A., Herwegh, M., Evans, B., Pfiffner, A., Austin, N. & Vennemann, T. 2007a: Microfabrics in carbonate mylonites along a large-scale shear zone (Helvetic Alps). Tectonophysics 444(1–4), 1–26.
Ebert, A., Herwegh, M. & Pfiffner, A. 2007b: Cooling induced strain localization in carbonate mylonites within a large-scale shear zone (Glarus thrust, Switzerland). Journal of Structural Geology 29(7), 1164–1184.
Epard, J. 1990: La nappe de Morcles au sud-ouest du Mont-Blanc, Mémoires de Géologie (Lausanne) 8, 165 pp.
Escher, A., Masson, H. & Steck, A. 1993: Nappe geometry in the Western Swiss Alps. Journal of Structural Geology 15(3–5), 501–509.
Etheridge, M. & Wilkie, J. 1981: An assessment of dynamically recrystallized grainsize as a palaeopiezometer in quartz-bearing mylonite zones. Tectonophysics 78, 475–508.
Evans, B., Renner, J. & Hirth, G. 2001: A few remarks on the kinetics of static grain growth in rocks. International Journal of Earth Sciences 90(1), 88–103.
Exner, H. 1972: Analysis of Grain- and Particle-Size Distributions in Metallic Materials. International Metallurgical Reviews 17(159), 25–42.
Frey, M., Teichmüller, M., Teichmüller, R., Mullis, J., Künzi, B., Breitschmid, A., Gruner, U. & Schwizer, B. 1980: Very low-grade metamorphism in external parts of the Central Alps: Illite crystallinity, coal rank and fluid inclusion data. Eclogae Geologicae Helvetiae 73, 173–203.
Gleason, G., Tullis, J. & Heidelbach, F. 1993: The role of dynamic recrystallization in the development of lattice preferred orientations in experimentally deformed quartz aggregates. Journal of Structural Geology 15(9–10), 1145–1168.
Goy-Eggenberger, D. 1998: Faible métamorphisme de la nappe de Morcles: minéralogie et géochimie PhD thesis, Université de Neuchâtel, Neuchâtel, 192 pp.
Groshong Jr, R., Pfiffner, O. & Pringle, L. 1984: Strain partitioning in the Helvetic thrust belt of eastern Switzerland from the leading edge to the internal zone. Journal of Structural Geology 6(1), 5–18.
Guillope, M. & Poirier, J. 1979: Dynamic recrystallization during creep of single-crystalline halite: An experimental study. Journal of Geophysical Research 84(B10), 5557–5567.
Hall, C. & Parmentier, E. 2003: Influence of grain size evolution on convective instability. Geochemistry, Geophysics, Geosystems 4(3), doi:10.1029/2002GC000308.
Handy, M. 1990: The solid-state flow of polymineralic rocks. Journal of Geophysical Research 95(B6), 8647–8661.
Handy, M. 1994: Flow laws for rocks containing two non-linear viscous phases: a phenomenological approach. Journal of Structural Geology 16(3), 287–301.
Harris, L., Burg, J. & Sauniac, S. 1983: Strain distribution within the Pardailhan Nappe (Montagne Noire, France) and structure of its basal thrust zone: implications for events associated with nappe emplacement. Journal of Structural Geology 5(3–4), 431–440.
Herwegh, M., Handy, M. & Heilbronner, R. 1997: Temperature-and strain-rate-dependent microfabric evolution in monomineralic mylonite: evidence from in situ deformation of norcamphor. Tectonophysics 280(1), 83–106.
Herwegh, M. 2000: A new technique to automatically quantify microstructures of fine grained carbonate mylonites: two-step etching combined with SEM imaging and image analysis. Journal of Structural Geology 22(4), 391–400.
Herwegh, M. & Kunze, K. 2002: The influence of nana-scale second phase particles on deformation of fine-grained calcite mylonites. Journal of Structural Geology 24, 1463–1478.
Herwegh, M. & Berger, A. 2003: Differences in grain growth of calcite: a field-based modeling approach. Contributions to Mineralogy and Petrology 145(5), 600–611.
Herwegh, M., Xiao, X. & Evans, B. 2003: The effect of dissolved magnesium on diffusion creep in calcite. Earth and Planetary Science Letters 212(3–4), 457–470.
Herwegh, M. & Berger, A. 2004: Deformation mechanisms in second-phase affected microstructures and their energy balance. Journal of Structural Geology 26(8), 1483–1498.
Herwegh, M., de Bresser, J. & ter Heege, J. 2005: Combining natural microstructures with composite flow laws: an improved approach for the extrapolation of lab data to nature. Journal of Structural Geology 27(3), 503–521.
Herwegh, M. & Pfiffner, O. 2005: Tectono-metamorphic evolution of a nappe stack: A case study of the Swiss Alps. Tectonophysics 404(1), 55–76.
Hobbs, B., Muhlhaus, H. & Ord, A. 1990: Instability, softening and localization of deformation. Geological Society London Special Publications 54(1), 143–165.
Humphreys, F. & Hatherly, M. 1995: Recrystallization and related annealing phenomena, Pergamon Tarrytown, NY, USA.
Humphreys, F. & Ardakani, M. 1996: Grain boundary migration and Zener pinning in particle-containing copper crystals. Acta materialia 44(7), 2717–2727.
Ji, S., Jiang, Z., Rybacki, E., Wirth, R., Prior, D. & Xia, B. 2004: Strain softening and microstructural evolution of anorthite aggregates and quartz-anorthite layered composites deformed in torsion. Earth and Planetary Science Letters 222(2), 377–390.
Kameyama, M., Yuen, D. & Fujimoto, H. 1997: The interaction of viscous heating with grain-size dependent rheology in the formation of localized slip zones. Geophysical Research Letters 24(20), 2523–2526.
Karato, S., Toriumi, M. & Fujii, T. 1980: Dynamic recrystallization of olivine single crystals during high-temperature creep. Geophysical Research Letters 7(9), 649–652.
Kennedy, L. & White, J. 2001: Low-temperature recrystallization in calcite: Mechanisms and consequences. Geology 29(11), 1027–1030.
Kirschner, D., Sharp, Z. & Masson, H. 1995: Oxygen isotope thermometry of quartz-calcite veins; unraveling the thermal-tectonic history of the subgreenschist facies Morcles Nappe (Swiss Alps). Bulletin of the Geological Society of America 107(10), 1145–1156.
Kirschner, D., Cosca, M., Masson, H. & Hunziker, J. 1996: Staircase 40 Ar/39 Ar spectra of fine-grained white mica; timing and duration of deformation and empirical constraints on argon diffusion. Geology 24(8), 747–750.
Kirschner, D., Masson, H. & Sharp, Z. 1999: Fluid migration through thrust faults in the Helvetic nappes (Western Swiss Alps). Contributions to Mineralogy and Petrology 136(1), 169–183.

Krabbendam, M., Urai, J. & van Vliet, L. 2003: Grain size stabilization by dispersed graphite in a high-grade quartz mylonite: an example from Naxos (Greece). Journal of Structural Geology 25(6), 855–866.
Kreemer, C., Haines, J., Holt, W., Blewitt, G. & Lavallee, D. 2000: On the determination of a global strain rate model. Earth Planets Space 52(10), 765–770.
Kreemer, C., Holt, W. & Haines, A. 2003: An integrated global model of present-day plate motions and plate boundary deformation. Geophysical Journal International 154(1), 8–34.
Loup, B. 1992: Mesozoic subsidence and stretching models of the lithosphere in Switzerland (Jura, Swiss Plateau and Helvetic realm). Eclogae Geologicae Helvetiae 85(3), 541–572.
Marquer, D., Petrucci, E. & Iacumin, P. 1994: Fluid advection in shear zones: evidence from geological and geochemical relationships in the Aiguilles Rouges Massif (Western Alps, Switzerland). Schweizerische Mineralogische und Petrographische Mitteilungen 74(1), 137–148.
Mas, D. & Crowley, P. 1996: The effect of second-phase particles on stable grain size in regionally metamorphosed polyphase calcite marbles. Journal of Metamorphic Geology 14(2), 155–162.
Mehl, L. & Hirth, G. 2008: Plagioclase recrystallization and preferred orientation in layered mylonited: Evaluation of flow laws for the lower crust. Journal of Geophysics Research, 113 B05202 doi: 10.1029/2007 JB005075.
Milton, N. & Williams, G. 1981: The strain profile above a major thrust fault, Finnmark, N Norway. Geological Society London Special Publications 9(1), 235.
Montesi, L. & Zuber, M. 2002: A unified description of localization for application to large-scale tectonics. Journal of Geophysical Research 107(B3), doi: 10.1029/2001JB000465.
Montesi, L.& Hirth, G. 2003: Grain size evolution and the rheology of ductile shear zones- From laboratory experiments to postseismic creep. Earth and Planetary Science Letters 211(1), 97–110.
Nes, E., Ryum, N. & Hunderi, O. 1985: On the Zener drag. Acta Metallurgica 33, 11–22.
Olgaard, D. & Evans, B. 1986: Effect of second-phase particles on grain growth in calcite. Journal of the American Ceramic Society 69(11), 272–277.
Panien, M., Schreurs, G. & Pfiffner, A. 2005: Sandbox experiments on basin inversion: testing the influence of basin orientation and basin fill. Journal of Structural Geology 27(3), 433–445.
Paterson, M. 1979: Deformation Mechanisms in Carbonate Crystals. Physics of Materials (A festschrift for Dr. Walter Boas), CSIRO and University of Melbourne, Melbourne, 199–208.
Paterson, M. 1995: A theory for granular flow accommodated by material transfer via an intergranular fluid. Tectonophysics 245(3–4), 135–151.
Pfiffner, O. A. 1981: Fold-and-thrust tectonics in the Helvetic Nappes (E Switzerland). Geological Society London Special Publications 9(1), 319–327.
Pfiffner, O. A. 1982: Deformation mechanisms and flow regimes in limestone from the Helvetic zone of the Swiss Alps. Journal of Structural Geology 4(4), 429–442.
Pfiffner, O. A. 1993: The structure of the Helvetic nappes and its relation to the mechanical stratigraphy. Journal of Structural Geology 15(3–5), 511–521.
Pieri, M., Burlini, L., Kunze, K., Stretton, I. & Olgaard, D. 2001a: Rheological and microstructural evolution of Carrara marble with high shear strain: results from high temperature torsion experiments. Journal of Structural Geology 23(9), 1393–1413.
Pieri, M., Kunze, K., Burlini, L., Stretton, I., Olgaard, D., Burg, J. & Wenk, H. 2001b: Texture development of calcite by deformation and dynamic recrystallization at 1000K during torsion experiments of marble to large strains. Tectonophysics 330(1), 119–140.
Poirier, J. 1980: Shear localization and shear instability in materials in the ductile field. Journal of Structural Geology 2(1–2), 135–142.
Ramsay, J. 1981: Tectonics of the Helvetic Nappes. Geological Society London Special Publications 9(1), 293.
Ramsay, J., Casey, M. & Kligfield, R. 1983: Role of shear in development of the Helvetic fold-thrust belt of Switzerland. Geology 11(8), 439–442.
Ramsay, J. 1989: Fold and fault geometry in the western Helvetic nappes of Switzerland and France and its implication for the evolution of the arc of the western Alps. Geological Society London Special Publications 45(1), 33–45.
Renner, J., Evans, B. & Siddiqi, G. 2002: Dislocation creep of calcite. Journal of Geophysical Research 107, 1–16.
Renner, J., Siddiqi, G. & Evans, B. 2007: Plastic flow of two-phase marbles. Journal of Geophysical Research 112, B07203, doi:10.1029/2005JB004134.
Rutter, E. 1972: The influence of interstitial water on the rheological behaviour of calcite rocks. Tectonophysics 14, 13–33.
Rutter, E. 1995: Experimental study of the influence of stress, temperature, and strain on the dynamic recrystallization of Carrara marble. Journal of Geophysical Research 100(B12), 24651–24664.
Rutter, E. 1999: On the relationship between the formation of shear zones and the form of the flow law for rocks undergoing dynamic recrystallization. Tectonophysics 303(1), 147–158.
Rutter, E. H., Casey, M. & Burlini, L. 1994: Preferred crystallographic orientation development during the plastic and superplastic flow of calcite rocks. Journal of Structural Geology 16(10), 1431–1446.
Rybacki, E., Paterson, M., Wirth, R. & Dresen, G. 2003: Rheology of calcite-quartz aggregates deformed to large strain in torsion. Journal of Geophysical Research 108, NO. B2, 2089, doi:10.1029/2002JB001833.
Sakai, T. & Jonas, J. 1984: Dynamic recrystallization-Mechanical and microstructural considerations. Acta Metallurgica 32, 189–209.
Schenk, O., Urai, J. & Evans, B. 2005: The effect of water on recrystallization behavior and grain boundary morphology in calcite-observations of natural marble mylonites. Journal of Structural Geology 27(10), 1856–1872.
Schmid, S., Boland, J. & Paterson, M. 1977: Superplastic flow in fine-grained limestone. Tectonophysics 43(3–4), 257–291.
Schmid, S., Paterson, M. & Boland, J. 1980: High temperature flow and dynamic recrystallization in Carrara marble. Tectonophysics 65, 245–280.
Schmid, S., Casey, M. & Starkey, J. 1981: The microfabric of calcite tectonites from the Helvetic Nappes (Swiss Alps). Geological Society London Special Publications 9(1), 151.
Schmid, S., Panozzo, R. & Bauer, S. 1987: Simple shear experiments on calcite rocks: rheology and microfabric. Journal of Structural Geology 9(5–6), 747–778.
Shimizu, I. 1998: Stress and temperature dependence of recrystallized grain size: A subgrain misorientation model. Geophysical Research Letters 25(22), 4237–4240.
Shimizu, I. 1999: A stochastic model of grain size distribution during dynamic recrystallization. Philosophical Magazine A 79(5), 1217–1231.
Siddans, A. 1983: Finite strain pattern in some Alpine nappes. Journal of Structural Geology 5(3–4), 441–448.
Skemer, P., Katayama, I., Jiang, Z. & Karato, S. 2005: The misorientation index: Development of a new method for calculating the strength of lattice-preferred orientation. Tectonophysics 411(1), 157–167.
Smith, C. 1948: Grains, phases, and ainterfaces: as interpretation of microstructure. Transactions of the American Institute of Mining and Metallurgical Engineers 15(4), 1–37.
Stipp, M., Stunitz, H., Heilbronner, R. & Schmid, S. 2001: Dynamic recrystallization of quartz: correlation between natural and experimental conditions. Geological Society London Special Publications 200(1), 171–190.
Ter Heege, J., De Bresser, J. & Spiers, C. 2002: The influence of dynamic recrystallization on the grain size distribution and rheological behaviour of Carrara marble deformed in axial compression. Deformation Mechanisms, Rheology and Tectonics Current Status and Future Perspectives, Special Publication Geological Society of London 200, 119–136.
Ter Heege, J., De Bresser, J. & Spiers, C. 2004: Composite flow laws for crystalline materials with log-normally distributed grain size: theory and application to olivine. Journal of Structural Geology 26(9), 1693–1705.
Ter Heege, J., De Bresser, J. & Spiers, C. 2005: Dynamic recrystallization of wet synthetic polycrystalline halite: dependence of grain size distribution on flow stress, temperature and strain. Tectonophysics 396(1–2), 35–57.

Trümpy, R. 1973: The timing of orogenic events in the Central Alps. Gravity and Tectonics"(De Jong, K. & Scholten, R.). Wiley, New York, 229–251.
Twiss, R. 1977: Theory and applicability of a recrystallized grain size paleopiezometer. Pure and Applied Geophysics 115(1), 227–244.
Twiss, R. & Sellars, C. 1978: Limits of applicability of the recrystallized grain size geopiezometer. Geophysical Research Letters 5(5), 337–340.
Underwood, E. 1970: Quantitative Stereology. Reading, MA, Addison-Wesley Publishing Co.
Urai, J., Means, W. & Lister, G. 1986: Dynamic recrystallization of minerals. AGU Geophysical Monograph 36, 161–199.
van der Wal, D., Chopra, P., Drury, M. & Fitzgerald, J. 1993: Relationships between dynamically recrystallized grain size and deformation conditions in experimentally deformed olivine rocks. Geophysical Research Letters 20(14), 1479–1482.
Walker, A., Rutter, E. & Brodie, K. 1990: Experimental study of grain-size sensitive flow of synthetic, hot-pressed calcite rocks. Geological Society London Special Publications 54(1), 259 pp.
Wang, Z., Bai, Q., Dresen, G., Wirth, R. & Evans, B. 1996: High-temperature deformation of calcite single crystals. Journal of Geophysical Research 101(B9), 20377–20390.
Warren, J. & Hirth, and G. 2006: Grain size sensitive deformation mechanisms in naturally deformed peridotites. Earth and Planetary Science Letters 248(1–2), 438–450.
Wenk, H., Venkitasubramanyan, C., Baker, D. & Turner, F. 1973: Preferred orientation in experimentally deformed limestone. Contributions to Mineralogy and Petrology 38(2), 81–114.
Xiao, X. & Evans, B. 2003: Shear-enhanced compaction during non-linear viscous creep of porous calcite-quartz aggregates. Earth and Planetary Science Letters 216(4), 725–740.

Manuscript received November 12, 2007
Revision accepted March 19, 2008
Published Online first July 25, 2008
Editorial Handling: S. Schmid, S. Bucher